Microscopy, Electrochemistry, and Conductivity Analyzer (MECA)
Phoenix Scout Mission for 2007
Microscopy Calibration Report

National Aeronautics and
Space Administration

JPL

Jet Propulsion Laboratory
California Institute of Technology
Pasadena, California

REFERENCES

No.	Item	Author	Date
1.	JGR paper " Microscopy capabilities of the MECA"	M. Hecht et al.	1/15/08
2.	Phoenix 2007 EM OM Calibration Evaluation Report	P. Woida	5/17/05
3.	Microscopy V&V Report	M. Hecht et al.	7/16/07
4.	Outline MECA AFM Calibration Report	D. Parrat, U. Staufer	7/10/07
5.	End Item Data Package for the UV Calibration and Magnetic substrates	M. Madsen et al.	11/30/05

LIST OF CHANGES

No.	Section	Item	Date
1.	I.1.2	Height for OM 69 added. Also some modifications in the text.	04/21/2008
2.	III.1	Axes in the schematic of the AFM scan	04/23/2008
3.	II.9	LED calibration on Mars, added	11/16/2008
4.	III.6.3	Calibration results (added)	03/27/2009

Table of Contents

MECA Microscopy Calibration Report

Acronym List

AFM	Atomic Force Microscope
ATLO	Assemble Test and Launch Operations
CC&C	Calibration, Characterization, and Cataloging
CCD	Charge-Coupled Device
CME	Control and Measurement Electronics
CRB	CCD Readout Board
EM	Engineering Model
EQM	Engineering Qualification Model
FM	Flight Model
FS	Flight Spare model
IMT	Institute of Microtechnology (Univ. Neuchatel)
JPL	Jet Propulsion Laboratory
LM	Lockheed Martin
LED	Light-Emitting Diode
MECA	Microscopy, Electrochemistry, Conductivity Analyzer
MPS	Max Planck Institute for Solar System Research
OM	Optical Microscope
PACI	Payload and Attitude Control Interface
PIT	Payload Interoperability Testbed
RAC	Robotic Arm Camera
SWTS	Sample Wheel & Translation Stage
TBD	To Be Determined
TBR	To Be Revised
UA	University of Arizona
UV	Ultraviolet

Document Overview & Scope

This report describes the calibration of the three components of the MECA microscopy station, i.e. the Optical Microscope (OM), the Atomic Force Microscope (AFM), and the Sample Wheel and Translation Stage (SWTS).

For each component, it summarizes the calibration which was performed prior to launch, as well as the calibration which will be needed on Mars in order to optimize the performances of the instruments and interpret the returned data.

This document will be a reference for the MECA team and the Phoenix Science team during and after the operations.

I.   Sample Wheel and Translation Stage (SWTS)

I.0.   Overview

The two-degree-of-freedom SWTS rotates to select a set of substrates for sample deposition or a portion of a single substrate for imaging. It translates to position the sample wheel outside the MECA enclosure to accept soil specimens from the robotic arm, to remove excess dirt by dragging the sample a metered distance under a blade, to focus the substrates for imaging, and to effectuate a coarse approach to the AFM. The SWTS is moved by a pair of stepping motors such that, in the absence of slipping, a simple count of the commanded steps determines the position. Dual limit switches are incorporated into the sample wheel rotation and the stage translation to prevent overdriving, to indicate the position at the ends of the translation sequence, and to indicate a reference position for the wheel. The SWTS fits within a 16 cm long by 12 cm wide by 12 cm tall envelope, including the AFM mount. It weighs just over 1 kg.

The SWTS must have sufficient mechanical and thermal stability to allow reproducible high resolution imaging and to retain the substrates and calibration standards such that their front surfaces are in a well-defined position relative to the microscope. It must allow for substrate illumination, mounting, and alignment to both the AFM and the optical microscope. It is designed to minimize cross-contamination of substrates and to protect delicate portions of the instrument until it is deployed on the surface of Mars.

Laboratory calibration of the SWTS consisted of confirming the relationship between stepping motor steps and distance traveled (rotation and translation); precisely determining the position of each limit switch; measuring backlash; and mapping the precise position of each substrate, both in translation and rotation.

I.1.   Positions along the translation axis

For translation of the SWTS, extension, or "outward", is defined as the direction that moves the sample wheel out of the box for sample delivery. Retraction, or "inward", moves the sample towards the microscopes. From the point at which the wheel touches the inside edge of the enclosure, an extension of 5 mm completely exposes the substrates after passing them under the leveling/scraping blade mounted on the enclosure. Retraction of just under 10 mm from the fully extended position brings the substrates back inside the box to the focal position.

I.1.1. Limit switches

The exact positions of all the limit switches were determined on the FM and stored in the MECA Parameters table. The stage translation axis is initialized at a step count of 10,000 at the point at which the OUT limit switch engages when the stage is moving out. The SAFE-TO-ROTATE limit switch indicates the position where the wheel can rotate without touching the AFM chip or the MECA enclosure. The FOCUS limit switch

indicates the coarse focus position for the OM. **Table 1. Positions where the limit switches change their state (in steps).**Table 1 gives an overview of those positions, with margins.

Table 1. Positions where the limit switches change their state (in steps).

OUT limit switch goes on	10000 ± 400
OUT limit switch goes off	10274 ± 400
SAFE limit switch goes off	44664 ± 400
SAFE limit switch goes on	45124 ± 400
FOCUS limit switch goes off	49311 ± 400
FOCUS limit switch goes on	49511 ± 400

During the characterization phase, and on a regular basis, the exact positions of the limit switches will be checked by initializing the stage.

I.1.2. Optical focus positions

As the heights of the substrates are not exactly the same, the optical focus position is different for each substrate. In ALTO, three surveys of the FM wheel were performed to determine the focus position of each substrate. The first survey was performed 500 steps (125 microns) outward of FOCUS_LS_ON, the second one 700 steps (175 microns) outwards, and the third one 900 steps (225 microns) outwards. Table 2 gives the estimated distance between the FOCUS limit switch (going on) and the optical focus position for each substrate, based on the best focalization among the three surveys. This information is stored in the MECA Coupon table and is used by the FSW to adjust the imaging position for each substrate. Approaching the substrates with the AFM ("static touches") will allow determining the exact position of the substrates.

The imaging positions depend also on the height of material deposited on the substrates. The leveling blade, which rides slightly above the surface of the wheel, is designed to limit the particle size to 0.2 mm, with 0.025 mm tolerance in the alignment of the substrate surfaces to the wheel surface. With the exception of magnetic substrates, which scavenge loose particles, this strategy limits the sample particles to project no more than 0.2 mm above the nominal front surface position of the substrates (see also I.1.3).

On the strong magnet, piles nearly 1 mm high have been observed, while 0.5 mm piles have been observed on the weak magnet. Thus, for those substrates, the optical focus position is moved outwards, in order to protect the AFM chip. Once OM images have been taken, the imaging position can be adjusted.

Table 2. Distance (in microns) between FOCUS_LS_ON and the optical focus position, given for each substrate. Multiplying these values by 4 gives the distance in motor steps.

Substrate	Correction	Substrate	Correction	Substrate	Correction
OM1	175	OM24	175	OM47	175
OM2	175	OM25	175	OM48	175
OM3	125	OM26	125	OM49	125
OM4	125	OM27	125	OM50	125
OM5	125	OM28	125	OM51	125
OM6	125	OM29	125	OM52	125
OM7	125	OM30	125	OM53	125
OM8	125	OM31	125	OM54	125
OM9	125	OM32	125	OM55	125
OM10	125	OM33	125	OM56	125
OM11	125	OM34	125	OM57	125
OM12	125	OM35	125	OM58	125
OM13	125	OM36	125	OM59	125
OM14	125	OM37	125	OM60	125
OM15	125	OM38	125	OM61	125
OM16	125	OM39	125	OM62	125
OM17	225	OM40	225	OM63	225
OM18	225	OM41	225	OM64	225
OM19	175	OM42	175	OM65	175
OM20	175	OM43	175	OM66	175
OM21	175	OM44	175	OM67	175
OM22	175	OM45	175	OM68	175
OM23	175	OM46	175	OM69	175

I.1.3. AFM_near position

In addition to the dual limit switches described in I.1.1, the position of the active AFM tip along the translation axis is interpreted by the stage as a limit switch. If the AFM is properly initialized, the AFM electronics informs the CME FPGAs when the stage goes in contact with the active tip, which immediately stops the motion. This serves both as a protection for the AFM and as a way to bring safely the surface in contact with the AFM before starting a scan.

The position of AFM_near was found during ATLO to be at 51160 for the first tip, as a stage motion was prematurely stopped when reaching this position. During the AFM approach procedure, the FSW tries to reach the AFM_near position, starting the translation from the FOCUS_LS_ON position. For the first tip, the limit for the number of steps being performed to find AFM_near should be set close to 500 microns (= (51160-49511)/4 + margin). Note that the position found in ATLO was not checked by running the AFM.

I.2. Positions along the rotational axis

For the rotation axis, clockwise (CW) and counter-clockwise (CCW) are defined for the viewer looking at the sample wheel from the top. The stage rotation axis 0 is defined as the point at which the rotation limit switch first becomes asserted when the stage is moving in the clockwise direction (see Table 3**Table 3. Positions where the rotation limit switch changes it state (in steps).**). Moving clockwise increases the rotation position according to motor step counts; moving counter-clockwise decreases the rotation position.

Table 3. Positions where the rotation limit switch changes it state (in steps).

Switch goes on (CW)	0 ± 100
Switch goes off (CW)	173 ± 100
Switch goes on (CCW)	173 ± 100

The 69 substrates are divided into ten sets of six, each of which can be exposed for soil delivery, and nine utility or calibration targets. Of the six substrates in each set, one is a uniform piece of silicone that remains pliant under martian conditions. The second is a custom micro-machined silicon substrate with posts and pits ("nanobuckets") that hold particles of an appropriate scale for AFM scanning. Two of the remaining four substrates are weak and strong magnets. The final two substrates are single "microbuckets" 3 mm in diameter and more than 2 mm deep, designed for OM imaging of bulk-like samples. Except for the microbuckets, each substrate has an exposed diameter of 3mm with 4.1 mm bases such that they can be flush mounted from behind the 3 mm opening. The gap between two substrates is 2 mm; the centers of two adjacent substrates are therefore distant by 5 mm.

The exact positions of the substrates have been determined on the FM wheel, and are kept in the MECA Coupon table. Table 4 gives the position of each substrate, as well as its type (SI = silicone, NB = nanobucket, WM = weak magnet, SM = strong magnet, MB = microbucket). The limit switch (position 0) is close to OM17 (tip breaking tool). A rotation of 360 deg corresponds to 24000 steps.

Table 4. Repartition and positions of the substrates on the FM sample wheel. The colors indicate the different sets (the calibration and utility substrates are in green).

ID	Mark	Type	Steps	ID	Mark	Type	Steps	ID	Mark	Type	Steps
OM1	26	WM	18744	OM24	55	SI	2411	OM47	84	WM	10077
OM2	27	SI	19077	OM25	56	NB	2744	OM48	85	SI	10411
OM3	28	NB	19411	OM26	57	MB	3077	OM49	86	NB	10744
OM4	31	MB	19744	OM27	58	SM	3411	OM50	87	MB	11077
OM5	32	SM	20077	OM28	61	MB	3744	OM51	88	SM	11411
OM6	33	MB	20411	OM29	62	WM	4077	OM52	1	MB	11744
OM7	34	WM	20744	OM30	63	SI	4411	OM53	2	WM	12077
OM8	35	SI	21077	OM31	64	NB	4744	OM54	3	SI	12411
OM9	36	NB	21411	OM32	65	MB	5077	OM55	4	NB	12744
OM10	37	MB	21744	OM33	66	SM	5411	OM56	5	MB	13077
OM11	38	SM	22077	OM34	67	MB	5744	OM57	6	SM	13411
OM12	41	MB	22411	OM35	68	WM	6077	OM58	7	MB	13744
OM13	42	tip cleaning tool	22744	OM36	71	SI	6411	OM59	8	WM	14077
OM14	43	AFM tip std	23077	OM37	72	NB	6744	OM60	11	SI	14411
OM15	44	AFM linear cal	23411	OM38	73	MB	7077	OM61	12	NB	14744
OM16	45	tip finder tool	23744	OM39	74	SM	7411	OM62	13	MB	15077
OM17	46	tip breaking tool	77	OM40	75	MB	7744	OM63	14	SM	15411
OM18	47	OM commem	411	OM41	76	WM	8077	OM64	15	MB	15744
OM19	48	OM linear cal	744	OM42	77	SI	8411	OM65	16	WM	16077
OM20	51	OM white cal	1077	OM43	78	NB	8744	OM66	17	SI	16411
OM21	52	OM UV cal	1411	OM44	81	MB	9077	OM67	18	NB	16744
OM22	53	MB	1744	OM45	82	SM	9411	OM68	21	MB	17077
OM23	54	WM	2077	OM46	83	MB	9744	OM69	22	SM	17411

I.3.   SWTS motions

I.3.1. Step size

The rotational step size of the wheel at the surface of the substrate is 15 µm, reproducible to within an OM pixel (3.9 µm) as determined by comparing OM images shifted by a known number of steps.

The translational step size of the FM SWTS is 0.25 µm, routinely reproduced to within a few steps as confirmed by measurement of the macroscopic separation of the limit switches. The fine step size is required in order to place the AFM tip near the center of its ~12 micron vertical range (i.e. normal to the sample, parallel to the translation direction) when it comes in contact with the surface.

This is accomplished by moving the sample wheel forward in 0.25µm steps and stopping on a signal from the AFM (see I.1.3). The smooth, fine translational motion is achieved in large measure by the use of flexures that link the fixed and translating part of the wheel.

It was determined at the IMT that the motion of the stage should be less than about 55 steps/sec to detect the contact before the tip crashes on the surface, and less than about 12 steps/sec to leave the tip in the middle of the vertical range after contact with the surface.

I.3.2. Stage speed

The speed of the stage can be varied by modifying the pulse width of the rotation or the translation (values between 100 and 20000). Table 5 shows the conversion between pulse width and steps per second. The nominal pulse width is 1000 for both rotation and translation, and a pulse width of 10000 is used for the AFM approach and retraction.

Table 5. Relation between pulse width and steps/s. The value in steps/s is obtained by multiplying the pulse width by 6.5E-6 and taking the inverse.

pulse width	steps/s
100	1538.46
500	307.69
1000	153.85
5000	30.77
10000	15.38
20000	7.69

I.3.3. Backlash compensation

As the wheel as some play in rotation, a strategy is used to compensate its effects when rotating to an absolute position. It consists of always doing the final motion to a substrate in the same direction (CW or CCW). Of course, this means that an overshoot has to be performed if the substrate is approached from the "wrong" direction. This overshoot has been estimated to be about 60 steps, and in general the counter-clockwise direction is preferred for the final approach.

I.3.4. Slippage in rotation

In June, 2006 the first survey of the PIT sample wheel was performed. The survey was done in 0.5 mm increments (33 or 34 steps), a full rotation of the wheel requiring therefore 720 movements. By analyzing the OM images, a significant slippage in a full circuit of the wheel was discovered, around 180 steps (2.25 mm). Since a full circuit of the wheel is 720 steps, it showed that the average slippage was 1 step per 4 moves. As the current FSW implementation moves the wheel in 1000-step increments, a full circuit of the wheel would result in a 6-step slip on average (0.15 mm), which would normally be acceptable.

However, the problem was presumably related to the fact that the motors were driven in 1-phase mode. Using the 2-phase mode of the motors (in April 2007), no slippage of any kind was observed – the SWTS traveled to the same endpoint and repeatedly returned to

the original baseline position (exactly!) over many trials. Note that the 2-phase operation gives 50% more torque at a cost of twice the power, but torque alone did not explain the problem observed in 2006. We are now using the 2-phase mode for the motion of the SWTS. In addition to the backlash compensation, this allows an accurate pointing on the sample wheel.

I.3.5. Change in height when translating

As an artifact of the flexures, the substrates dip downwards at the extremes of motion relative to the microscopes. In particular, the substrates will drop approximately 100 µm from the OM focus position to the AFM scan position, a useful characteristic because it prevents the region accessible to the AFM from being obscured by the cantilever in the OM image.

I.4. Calibration substrates

I.4.1. OM White Calibration Target

The white calibration target is used for the calibration of the color LEDs. Figure 1 shows two images of this target, one taken on the FM (left) and the other on the PIT (right). As the images taken on the FM in ATLO were clearly saturated for all colors, further tests were performed on the PIT with smaller exposure duration, determined for each color based on previous images. The new values (corrected for temperature based on Figure 18) will be used during the characterization phase as a coarse adjustment for the illumination. The final calibration will be performed by means of the images of this target taken on Mars.
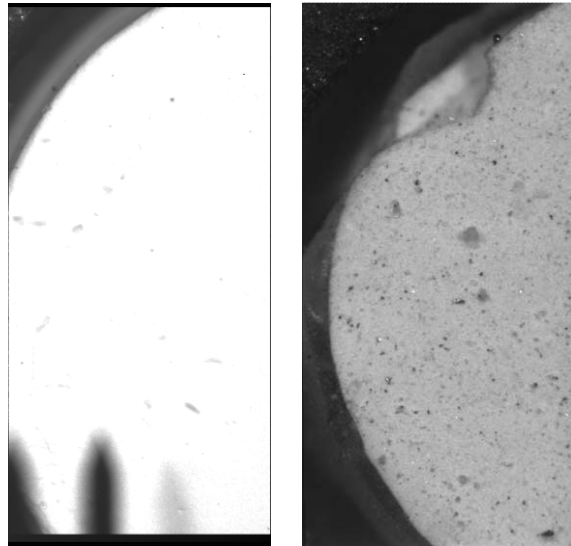
Figure 1. Left: OM image of the white calibration target taken in ATLO. The illumination consisted of the 3 red LEDs (325 counts, i.e. 162.5 ms). This image was clearly saturated. Right: OM image of the white calibration target taken on the PIT. The illumination consisted of the 3 red LEDs, with a corrected duration (131 counts, i.e. 65.5 ms). This image is not saturated.

I.4.2. OM UV Calibration Target

The UV calibration target is a tablet of $BaMgAl_{10}O_{17}:Eu^{2+}$ (BAM) prepared by Eugenius Zych, Univ. of Wroclav, Poland using a process of pressing and sintering at 1750 °C for 15 h. Photophysical properties are very similar to the pre-sintered powder and to the commercial powder (available, for example, from Philips Lighting Inc.).

Figure 2. BAM batch C422 seen in VIS (left image) and UV (254 nm, right image). Tablet #2 and #5 (from left to right) were selected as FS1 and FM1, respectively

BAM absorbs in the entire UV (220-440 nm) and has a comparatively flat excitation spectrum, especially in the spectral region 250-350 nm as shown in Figure 3. The decrease in excitation strength at wavelengths shorter than 250 nm is likely an artifact of the low intensity of the incoming radiation. Emission is from the Eu^{2+} ions by the decay process $4f^{6}5d \rightarrow 8S_{7/2}(4f^{7})$ and appears as a single broad peak centered at ~ 450 nm. The decay time constant is approximately 1100 ns. The quantum efficiency is greater than 50% and thus more than half of the incident UV photons are re-emitted as blue-green photons.
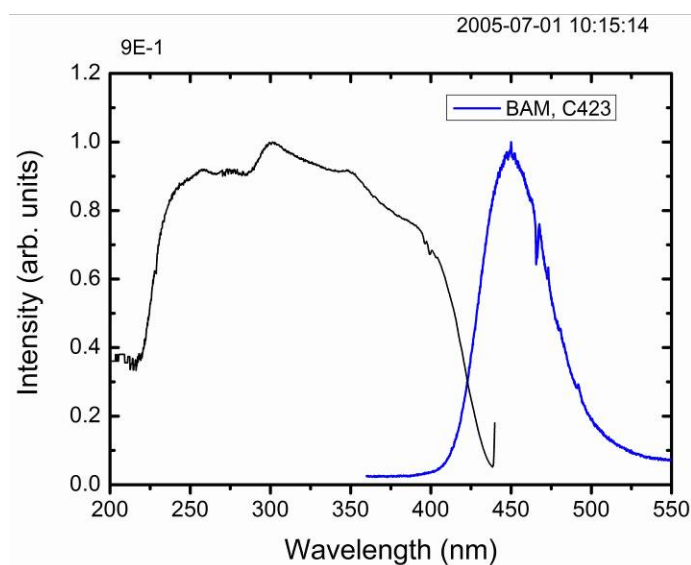
Figure 3. Excitation (left) and emission (right) spectra of flight-like BAM tablets.

Figure 4. shows the relative response of the UV target to illumination at a wavelength similar to that of the UV LED (images with the actual UV LEDs are essentially the same). Absolute QE, expected to be around 80%, is difficult to measure, so the image has been normalized to unity. Also note that the flight tablet has an irregular shape. This defect does not affect the performance of the material and helps align images of the mounted target to the pre-flight luminescence maps.
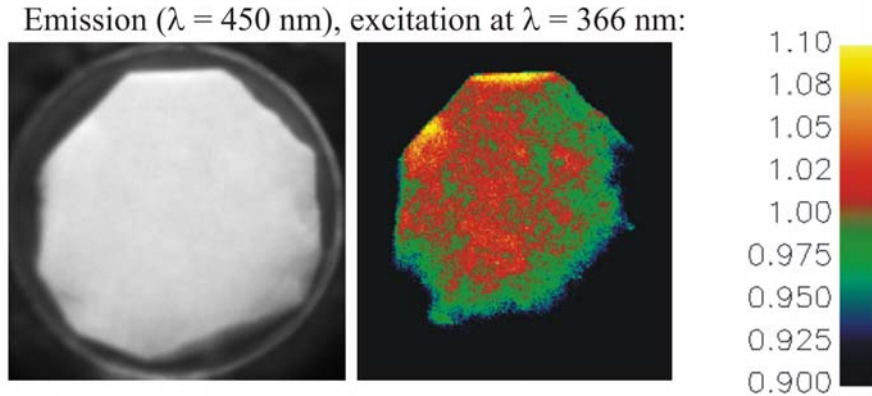

Figure 4. UV luminescence map of the response of the flight UV calibration target to illumination by UV radiation at 366nm. The color contour plots in are all normalized to unity, but the scale is proportional to the quantum efficiency of the luminescent tablet.

I.4.3. OM Linear Calibration Target

The standard linear calibration target (USAF 1951 standard) comprises lines, circles, squares, bars, and numbers. This target is used to determine the optical properties (see part II). Figure 5 shows a mosaic of two OM images of this substrate taken with red illumination.
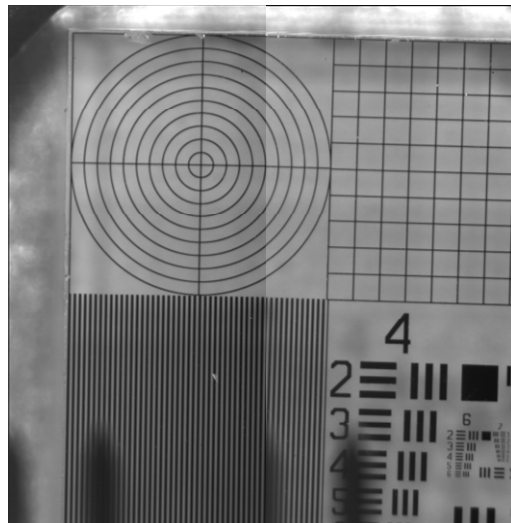

Figure 5. A mosaic of two adjacent images of the OM linear calibration substrate acquired with red LED illumination

I.4.4. OM Commemorative Target (or "stitching" target)

The commemorative target consists of microtext written on a silicon substrate to be used to assess the parameters for joining mosaics of adjacent images. It will be imaged on Mars during the characterization phase.

I.4.5. AFM Linear Calibration Substrate

On the left in Figure 6 is an SEM image of the AFM linear calibration standard (TGX1), which is represented by the manufacturer (NT-MDT) to have a pitch of 3 ± 0.05 μm and an edge curvature radius of less than 10 nm. This will be used to correct for the large saddle distortion typical of this type of AFM drive, and to establish an absolute length scale, which is expected to be a weak function of temperature (the scan size is reduced by 30% at -30°C relative to the size at room temperature). Details are given in III.6.1.1.
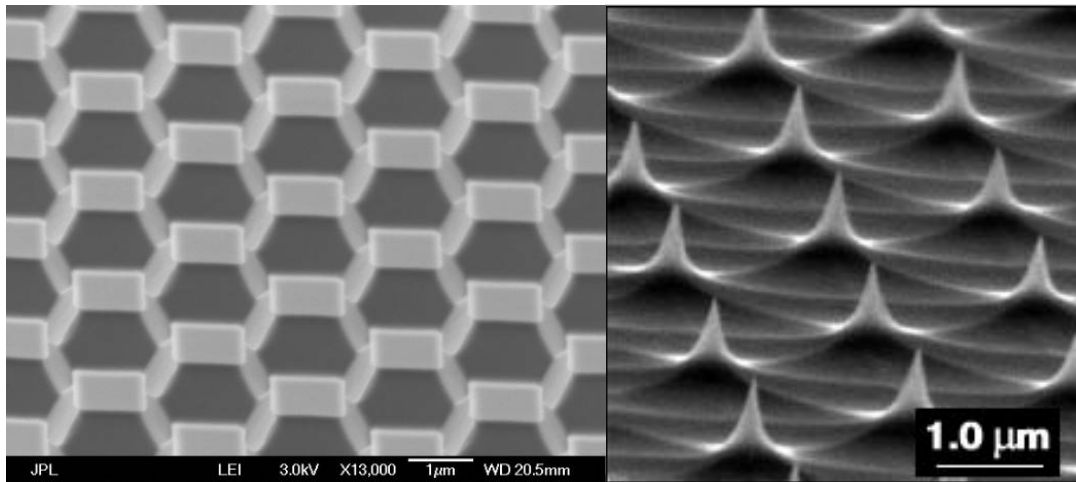
Figure 6. Left: SEM image of AFM linear calibration target. Right: SEM image of AFM Tip Standard (pincushion). Both are commercial products from NT-MTD.

I.4.6. AFM Tip Standard Substrate

On the right in Figure 6 is an SEM image of the AFM Tip Standard (pincushion) calibration substrate (TGX1) from the same vendor, consisting of an array of extremely sharp tips with 2.12 μm pitch (3.0 μm across the diagonal), 0.3 to 0.6 μm height, and curvature of less than 10 nm. Since these tips have a higher aspect ratio than the AFM tip itself, it will be used to characterize the AFM tip shape. Details are given in III.6.1.2.

I.4.7. Tip Finder Tool

The Tip Finder is a coded substrate designed by Surface/Interface, Inc. to have distinct features that allow registration on both the OM and the AFM scale. This will be used to register the AFM tip positions to the OM image, a critical step in AFM target selection. An SEM image of this target is shown in Figure 7. In order to determine the position of

the AFM tip relative in the OM field of view, an AFM image of 40 microns is required. An example of AFM image is given in III.6.1.3.
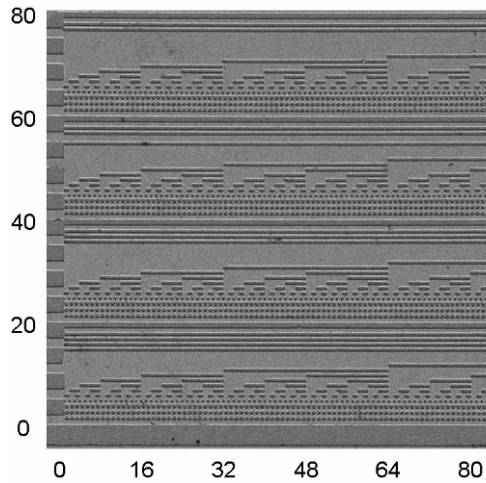

Figure 7. SEM image of a portion of the tip finder substrate. The number along x and y indicates the position (in microns) relative to the lower left corner.

I.5. Images of the substrates acquired in cruise

The first sample to be analyzed will be dust collected during landing, and will presumably represent surface material disturbed by the landing jets. In preparation for that event, four of the target substrates have been imaged in cruise (Figure 8) in order to verify their cleanliness and identify specific features (such as the fiber on the micromachined substrate) that should not be ascribed to the sample. They will be in the sample acquisition position during landing.
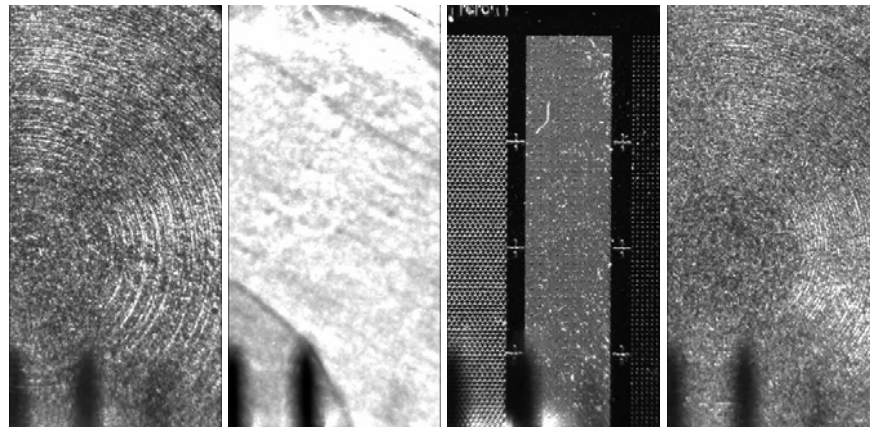
Figure 8. Monochrome OM images acquired in cruise of substrates that will be exposed during landing. From left to right, targets #59 (weak magnet), #60 (silicone), #61 (micromachined), and #63 (strong magnet).The fiber on the micromachined substrate was present at integration but could not easily be removed without damaging the substrate. The remainder of the set, the microbuckets in #58 and #62, were not imaged since the bottom can not be brought into focus when they are empty

II.   Optical Microscope (OM)

II.0.   Overview
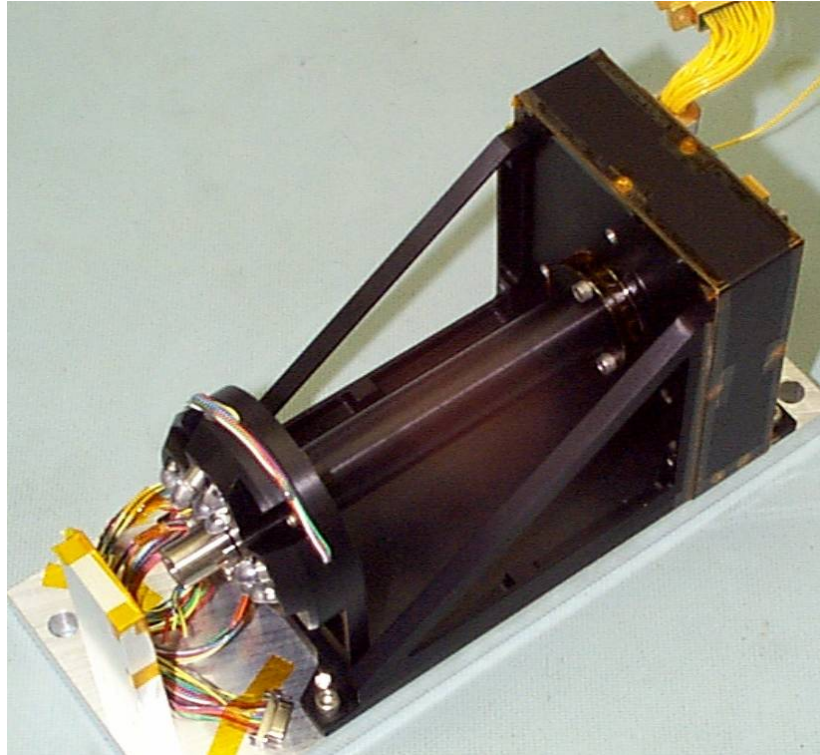
Figure 9. Engineering Model of the Optical Microscope.

The MECA optical microscope is a fixed-focus, fixed magnification optical system that sits in a horizontal orientation with a housing in the front containing two lenses surrounded by three banks of four LEDs – one each in red, green, blue, and ultraviolet – and a CCD assembly in the rear. Since the CCD itself is monochrome, color imaging is simulated by combining images acquired with red, green, and blue illumination. The UV LEDs radiate at ~375 nm with a visible light blocking filter and are used for fluorescence measurements only (the CCD is blind in the passband of the filter on the UV LED).

The Loral CCD is a 512 pixel square, with 512x256 pixels exposed for imaging and the remainder used for frame-transfer. Transfer of image charge to the storage section takes 0.5 ms and does not cause any measurable image degradation for the OM. The active pixel area is 17x23 μm, with a 23 μm pixel pitch. The rectangular area results from the incorporation of anti-blooming gates, which run vertically along the array. The CCD was mounted on a custom sensor head board by the Max Planck Institute for Solar System Research (MPS) and provided along with frame-buffering electronics to the University of Arizona for incorporation into the microscope as a contribution to the Phoenix mission.

Electronics for the CCD are shared with the Robotic Arm Camera (RAC). The chip is read out with a 12-bit analog-to-digital converter to provide an image data range of 0-4095 digital numbers (DN). Separate MECA electronics power the LEDs and the sample stage.

Prior to integration, the optical microscope was calibrated using custom rulings, targets, and integrating spheres to determine geometrical parameters (resolution, working distance, depth of field, and field of view), flat field correction, dark current levels, and the spectral output of the LEDs. While some of these parameters can be verified on the surface of Mars, it is generally assumed that these properties will not change significantly over the life of the instrument.

II.1. Resolution

The 10 μm line of the USAF 1951 standard shown in Figure 10 (Group 6, line 5) is readily resolved by the EM, as is the 10 μm separation of a precision Ronchi ruling (see II.3), suggesting a resolution better than 10 μm. See also II.2 for the resolution of the OM.
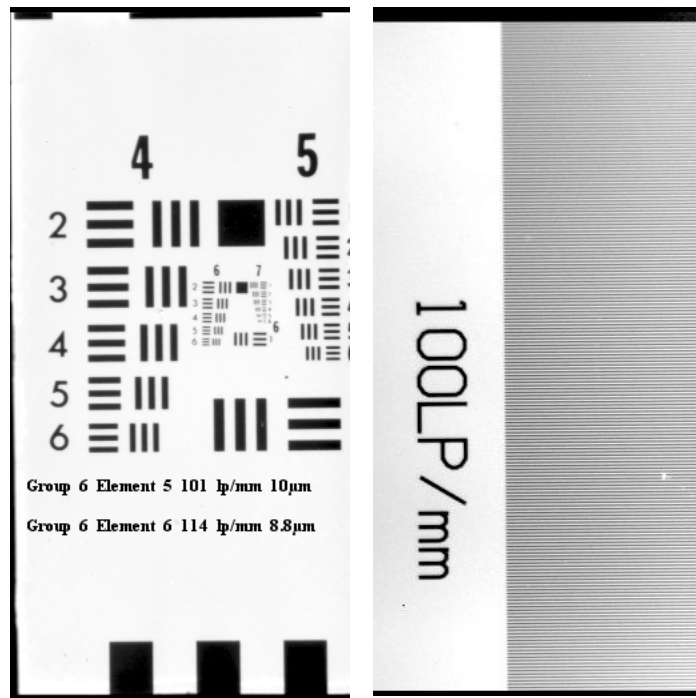
Figure 10. Left: EM OM calibration image of USAF 1951 Standard Target. Right: FM image of 0.01 mm linewidth Ronchi ruling

II.2. Field of view and aberrations

Field of view and possible spherical or astigmatic aberrations were studied using concentric circle targets bisected by a crosshair. Figure 11 shows the target used for calibration of the flight unit, featuring a 2.0mm OD, 0.1mm increment, and 7.5 µm line width, and Figure 12 a square grid target used to detect aberrations such as pincushioning and barreling. No significant optical image distortion can be seen across the 1x2 mm field of view, and resolution of the 5.0 µm line suggests that the microscope resolution is limited by the pixel size. This conclusion was subsequently confirmed by characterizing an identical optical system with a higher resolution CCD.
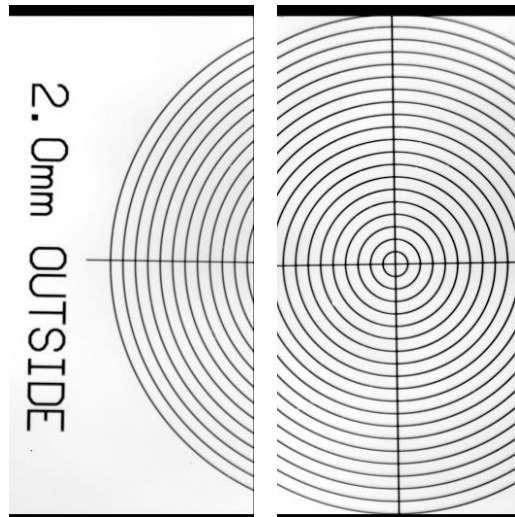
Figure 11. Left: Flight model OM image of target with 2.0mm OD, 0.1mm increments, 7.5 µm line width, positioned to show label. Right: the same target centered in the field.

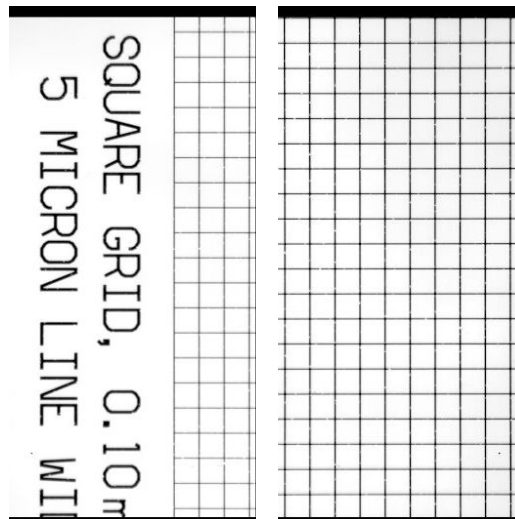*Figure 12. Bottom left: Flight model OM image of square grid with 0.1 mm spacing, 5 µm line width. Bottom right: the same target centered in the field.*

II.3. *Working distance and depth of field*

The working distance and the depth of field of both the EM and FM microscopes were calibrated at the University of Arizona using a Ronchi grating. A Ronchi grating is patterns of evenly spaced alternating clear and opaque lines. The lines and spaces have equal widths and are most commonly defined in terms of frequency either in line pairs per mm (lp/mm), or line pairs per inch (lpi). The Ronchi Rulings are used primarily for determining the MTF (Modulation Transfer Function) / maximum possible resolution and the maximum resolution for best acuity.

In order to determine the depth of field, the Ronchi grating was tilted at 10:1 such that the edges are intentionally out of focus (see Figure 13). A depth of field greater than 50 µm was measured by determining the extent of the in-focus region. This measurement also served to calibrate the best focus position and to confirm that the image plane is orthogonal to the OM axis. For the EM OM, the working distance showing the best focus was 13.88mm.
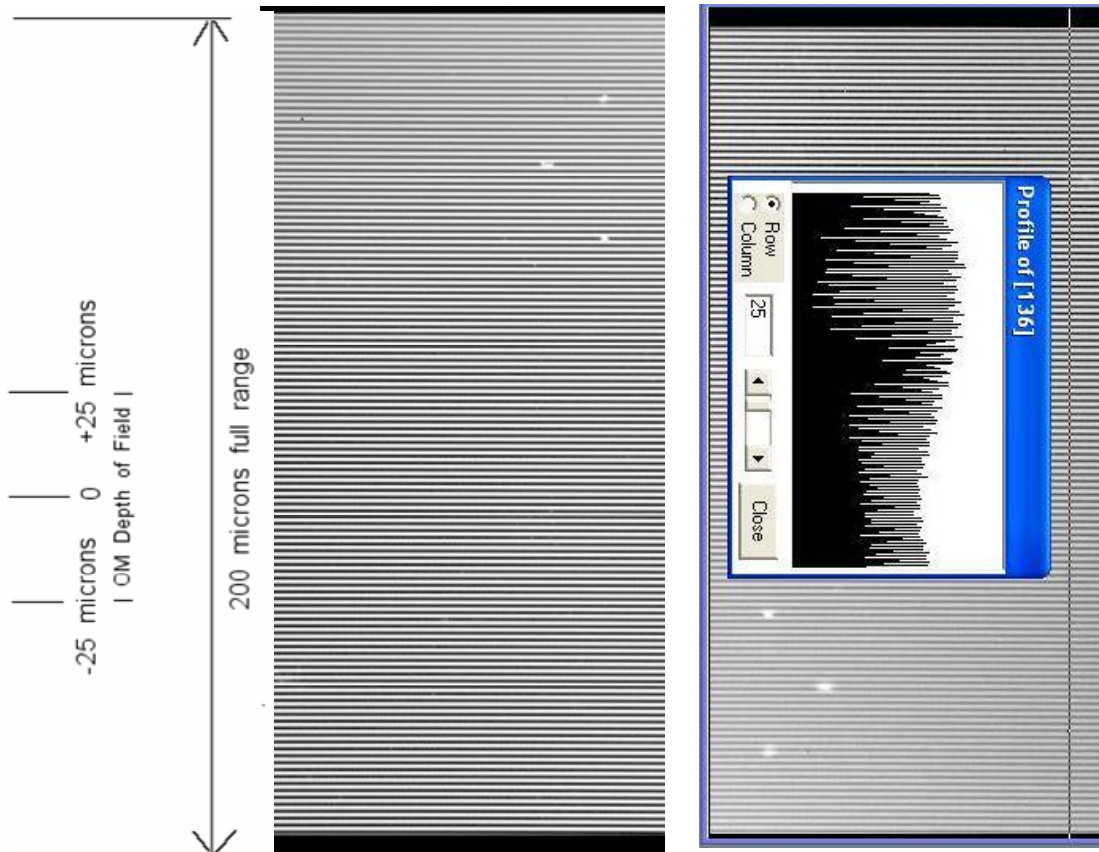

Figure 13. Flight model images of a 60LP/mm Ronchi Grating (16.67µm Period and 8.33 µm Line Width) angled at 10:1 such that the top of the image is 200 µm below the bottom across the 2 mm FOV; Left: Annotated image of grating with best focus in center. Good resolution and contrast is evident at the +/- 25µm marks; Right: Grating translated to focus at the extreme top to show the full range from focus to +200 µm. Modulation Transfer Function analysis is superimposed.

II.4. Full Aperture Relative Spectral Response

The OM focal plane array scheme is the same one used for the RAC. Data are returned with 12 bits/pixel. Typical exposure times are 0.3 to 0.7 s., depending on the selection of LEDs that provide the illumination. In general, the illumination strategy will be keyed to typical particle reflectivity rather than the reflectivity of the various substrates. The target signal to noise ratio is 200:1 for 100 msec exposure.

The spectral response of the optical and detector system was measured for the identical EM unit by filtering an integrated light source through an Acton SP-150 monochromator onto an integrating sphere, which was then calibrated by an Ocean Optics USB 2000 spectrometer . A series of full aperture images were acquired at over a 400nm -1000nm range at 5nm steps using a 5nm bandpass (see Figure 14). Each data point was derived from three live frames (512 x 256 x 12 bit), one dark frame using the same integration time, and a shutter frame (a single clock cycle with illumination on). The dark frame and shutter frames were subtracted from the average of the live frames.
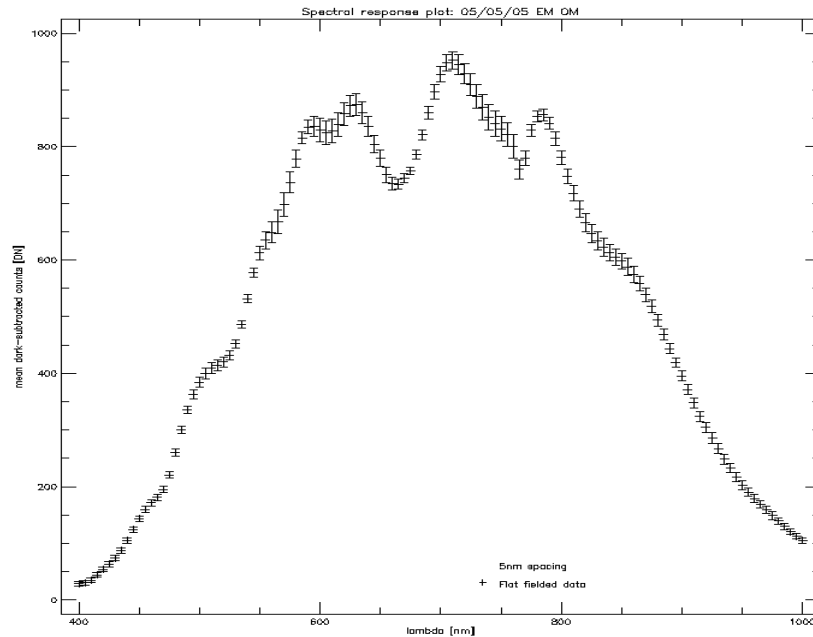

Figure 14. EM OM Spectral Response

II.5. Camera Linear Response

The OM Linear Response is done in two ways. One is to use the Acton SP-150 Monochronometer at each LED wavelength (II.5.1). The second is to locate a white target at focus and illuminate it with each triplet of LEDs (II.5.2).

II.5.1. Flat Field Linearity Test with Monochromator

A flat field correction for the optical and detector system was determined by using the Acton SP-150 monochromator at wavelengths corresponding to the four LED colors (375, 466, 543, and 636 nm). Integration times were varied by increments of 10% relative to a value empirically determined to be near full-well but with no saturated pixels. Unilluminated images were similarly acquired as a background reference (Figure 15).
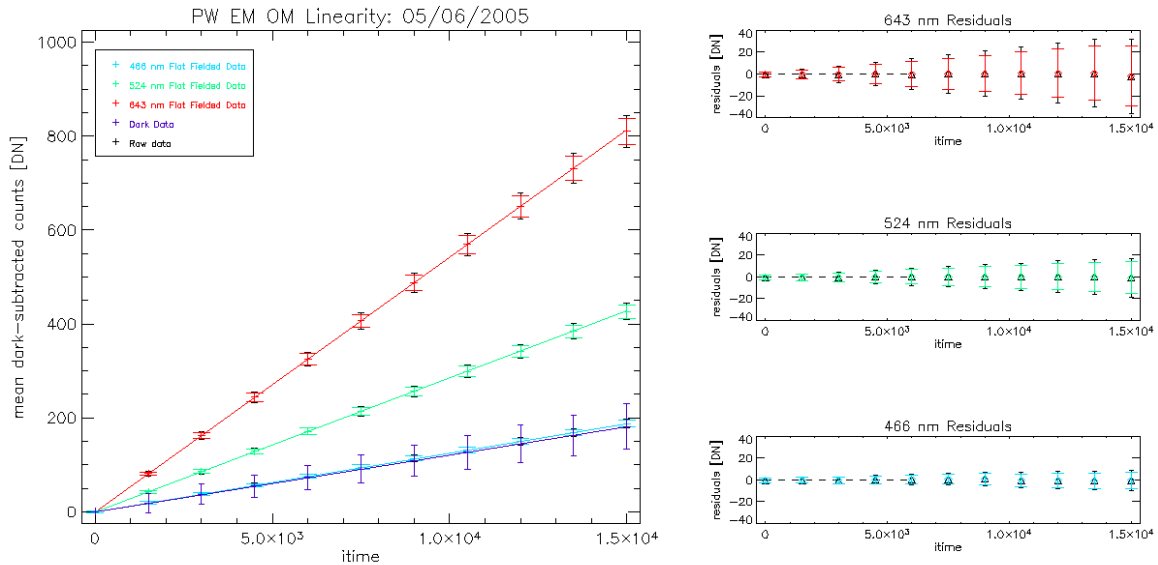

Figure 15. Three Color Linearity taken with a monochromator.

II.5.2. Flat Field Linearity Test with LEDs

In a separate measure of OM Linear Response, each of the twelve LEDs was individually focused on a flat Spectralon diffuser covered by a microscope slide. Images were then acquired as for the monochromator test.

The linear response of the red, green, blue, and ultraviolet LEDs was determined from images of a broadband optically reflective white Spectralon® from Labsphere, Inc. (a broadband optically reflective target formed from Teflon spheres), polished for uniformity. The 12-bit counter saturates at 4095 counts, limiting the acceptable exposure. A measure of image acquisition speed with the UV LED was derived from measurements of the LED composite spectrum acquired using an Ocean Optics USB 2000 Spectrophotometer. The integration time was 200 ms for the visible LEDs and and 1 second for the UV LEDs.
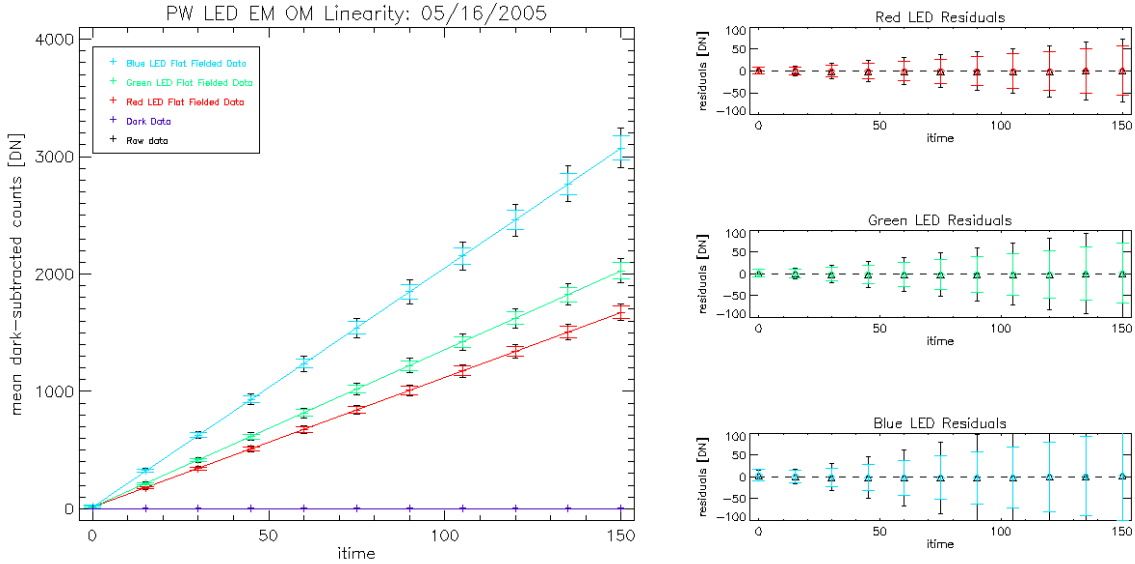
Figure **16** shows the linearity of the RGB LEDs with exposure time.
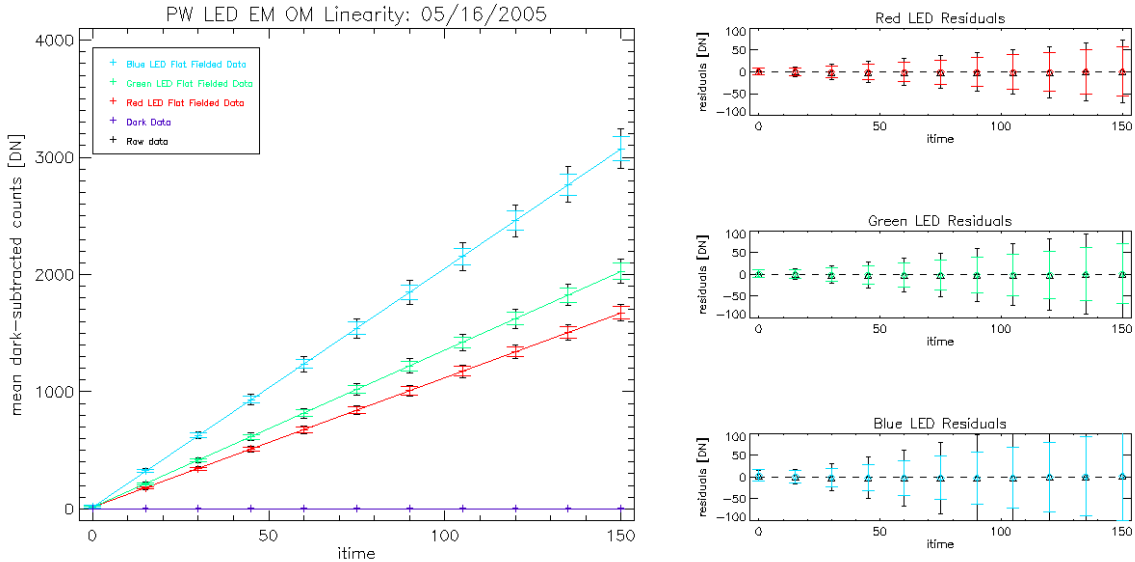

Figure 16. Three Color Linearity taken with Red, Green, and Blue LEDs.

II.6. LEDs Composite Spectral Output

Figure 17 shows the composite output spectrum of the LEDs, measured with a spectrometer coupled to an integrating sphere with a fiber optic. In more extensive tests of LEDs from the same lot it was determined that the LEDs do not change their peak wavelength as they warm up, but the bandwidth widens slightly. The UV LED has a filter to insure no shift in wavelength.
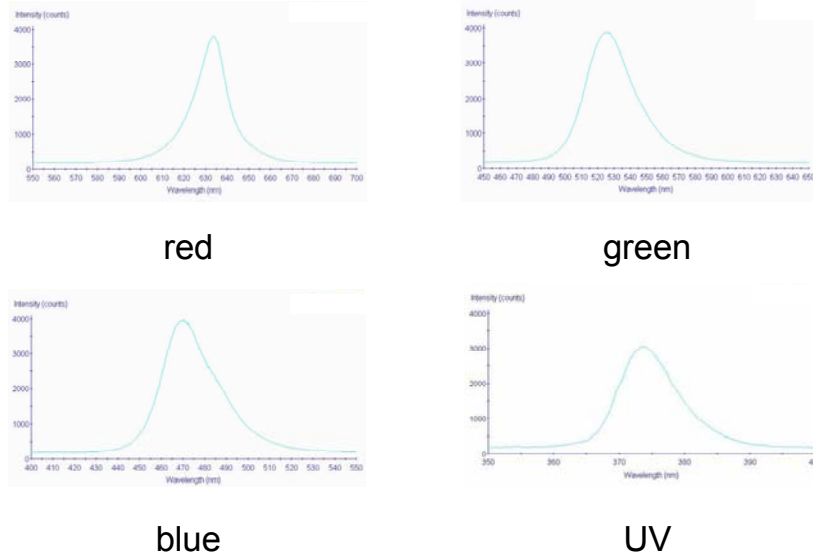
red

green

blue

UV

Figure 17. EM OM LED Composite Spectral Output as determine by the Ocean Optics USB2000 spectrometer. Integration time was 200 ms for red, green, and blue, and 1000 ms for UV, with all three LEDs illuminated for each color. Each curve is an average of 5 spectra.

II.7. **LEDs intensities with temperature**

The intensities of the LEDs vary with temperature. Figure 18 shows the subsequent variations in the responsivity of the OM camera to the blue, green and red LEDs. The responsivity at -20 deg C (near the mid-range of the operating temperatures), is 84 % of the one at room temperature for the red LED, 89 % for the green LED and 94 % for the blue LED. The exposure durations have to be adapted in consequence, and a finer adjustment was performed post-landing by imaging the OM white target (I.4.1) during the mission (see II.9).
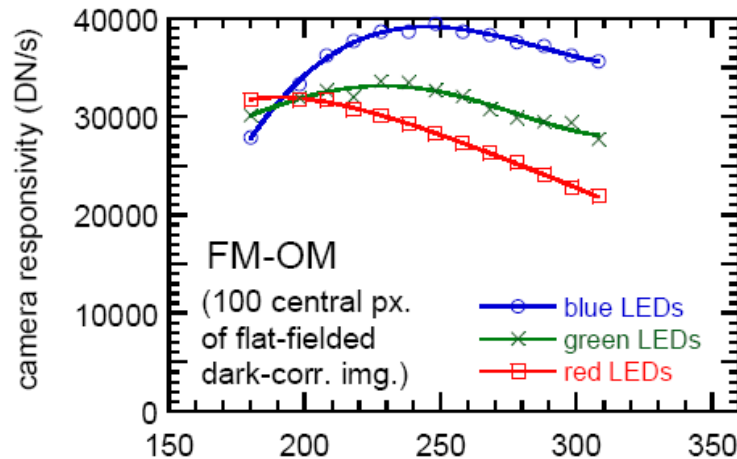

Figure 18. FM OM responsivity to the color LEDs with temperature (in K).

For the UV LED intensity, there is a steep slope just around operating temperatures. Figure 19 shows the curve for the Beagle 2 LED, which is very similar to those used for MECA. Based on this curve we can estimate that the intensity of the UV LEDs will decrease with a factor of about 1.5 at -20 deg C, compared to room temperature. A better calibration will be made by imaging the UV calibration target (see I.4.2) on Mars.
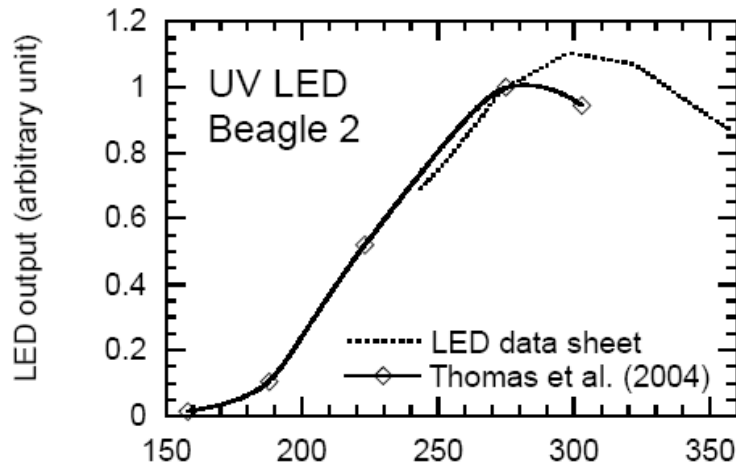

Figure 19. Output of the UV LEDs of Beagle 2 with temperature (in K).

II.8.   *Transmission spectrum of Schott filter GG420*

The OM is equipped with a 1mm thick Schott filter GG420. Using the transmission spectrum of a 3mm GG420 filter provided by the manufacturer, the transmission spectrum of the OM filter was calculated by taking the cube root. Figure 20 shows the transmission spectrum of the OM filter. By comparing this graph with Figure 17, one can see that almost 100% of the light from the UV LED will be absorbed by the filter. Thus, any particles visible under UV illumination must be fluorescing in the visible.
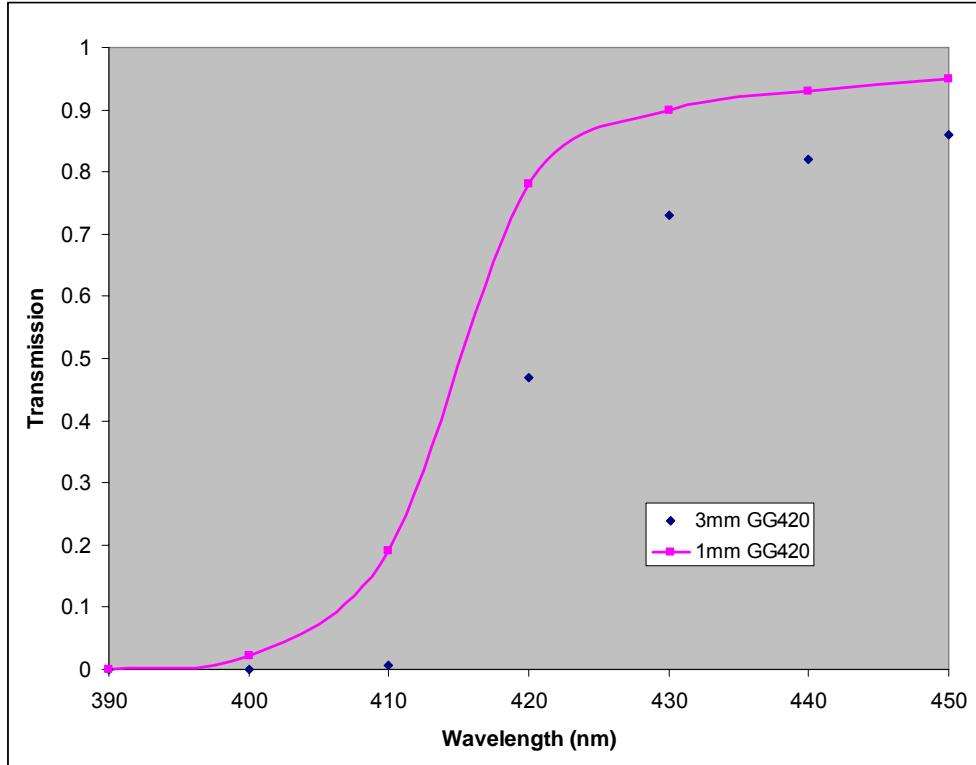
Figure 20. Transmission spectrum for the OM filter. The transmission is below 10^{-5} for wavelengths smaller than 390 nm.
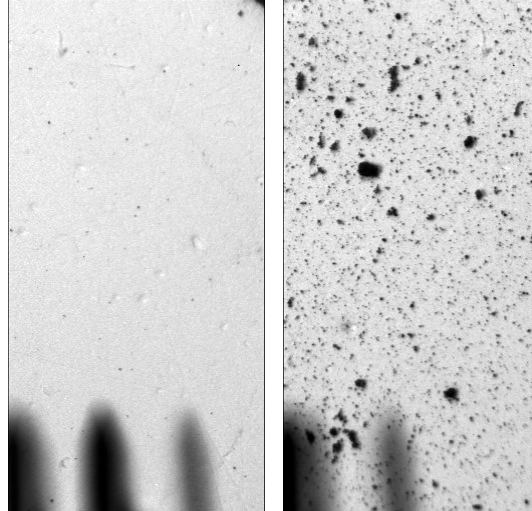
II.9.   LEDs calibration on Mars

The color LED intensities vary with the temperature (see in II.7), and also with time. In order to calibrate them, images of the white targets were taken several times during the mission, at different temperatures.

Color composites were created using images taken with each set of color LEDs (only 2 LEDs for each color, as the third blue LED caused reflection on the AFM cantilevers). Thus, we were especially interested in the relative intensity between the LEDs. The calibration consisted therefore in weighting each color image to obtain the correct color composite.

II.9.1. Method

The images of the white target were taken using exposure durations based on a coarse pre-launch calibration: **red_exp_calib** (usually 82.5ms), **green_exp_calib** (usually 71ms) and **blue_exp_calib** (usually 51ms).

Figure 21. OM images of the white calibration target taken on Mars, on sol 4 (left) and on sol 111 (right). Here the illumination consists of two blue LEDs. Some particles accumulated on the substrate. Between the 2 images, the first AFM tip was removed.

If this calibration was perfect, the obtained intensities should be the same with the red, blue and green illuminations. The intensity of each image was determined using the most occurring DN value (mode). That way, the apparition of contaminants on the target (see Figure 21) did not affect the measurements, as the coverage was relatively small relative to the remaining white area.

As we only had a coarse calibration, we found different intensities for each illumination: **I_red** (e.g. 1660 DN), **I_green** (e.g 1770 DN) and **I_blue** (e.g. 1460 DN). Thus, we needed correction factors to create the color composites.

Note that we used different exposure durations when taking images of the other substrates. In general, those durations were proportional to **red_exp** = 275ms, **green_exp** = 200ms and **blue_exp** = 162.5ms, with the exception of the images taken between sols 20 and 41 (too much red because of a problem in the VML library).

The correction factors are given by those formulas:
R_corr = (I_red)$^{-1}$ * red_exp_calib / red_exp
G_corr = (I_green)$^{-1}$ * green_exp_calib / green_exp
B_corr = (I_blue)$^{-1}$ * blue_exp_calib / blue_exp

There were then normalized such as **B_corr = 1.**

II.9.2. Results

Images of the white target were taken on sols 4, 57, 111, 117, 120, 121 and 137. For the green LED, it appeared that the relative intensity compared to the blue LEDs was only dependent on the temperature. For the red LEDs, the relative intensity was not only

dependent on the temperature, but also on the epoch of the mission. A possible explanation is that the blue and green LEDs generally increase their intensity with use, while it is the opposite for the red LEDs. After a certain number of cycles, the variations tend to decrease, reaching a kind of plateau. The red LEDs are also more sensitive to radiations.

The graph hereunder shows the corrections factors plotted with the temperature. Linear fitting is used for modeling. For the green LEDs, the model is valid for the whole mission. For the red LEDs, it's only valid for sols 111 to 137 (when the data were acquired).
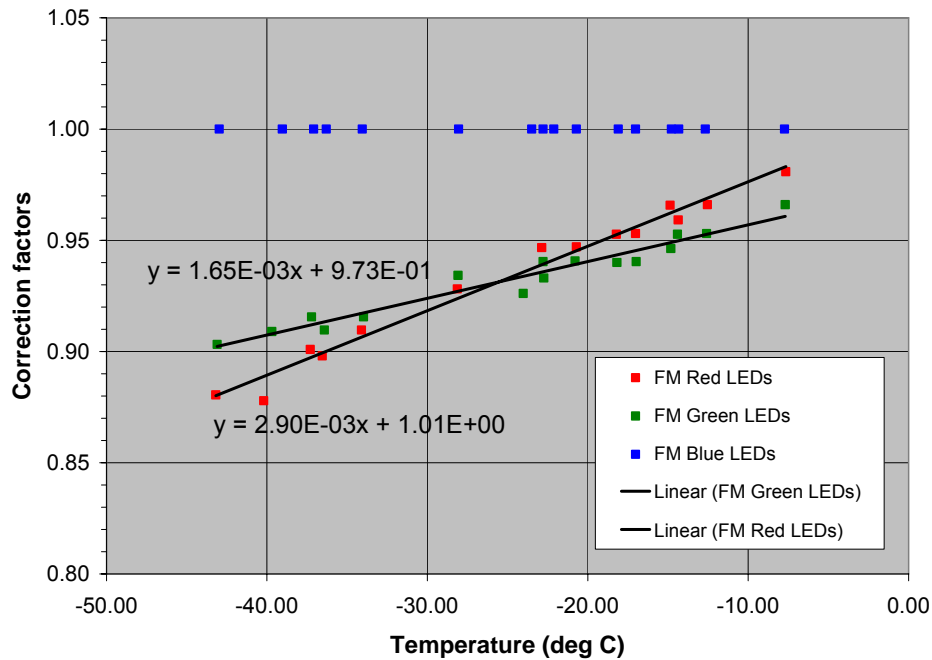

Figure 22. Correction factors with the temperature based on calibration measurements done on sols 111, 117, 120, 121 and 137. For those sols, the red correction factor is almost constant at a given temperature (variation < 1%).

In order to determine the red correction factors for the whole mission, it is reasonable to think that the variation in temperature can be separated from the variation in time, i.e. that R_corr(T, t) = f(T) * g(t) . That way, all results can be transposed in a correction at -23 deg C, and from there, the function g(t) can be determined. The resulting time dependency of R_corr is shown in Figure 23.
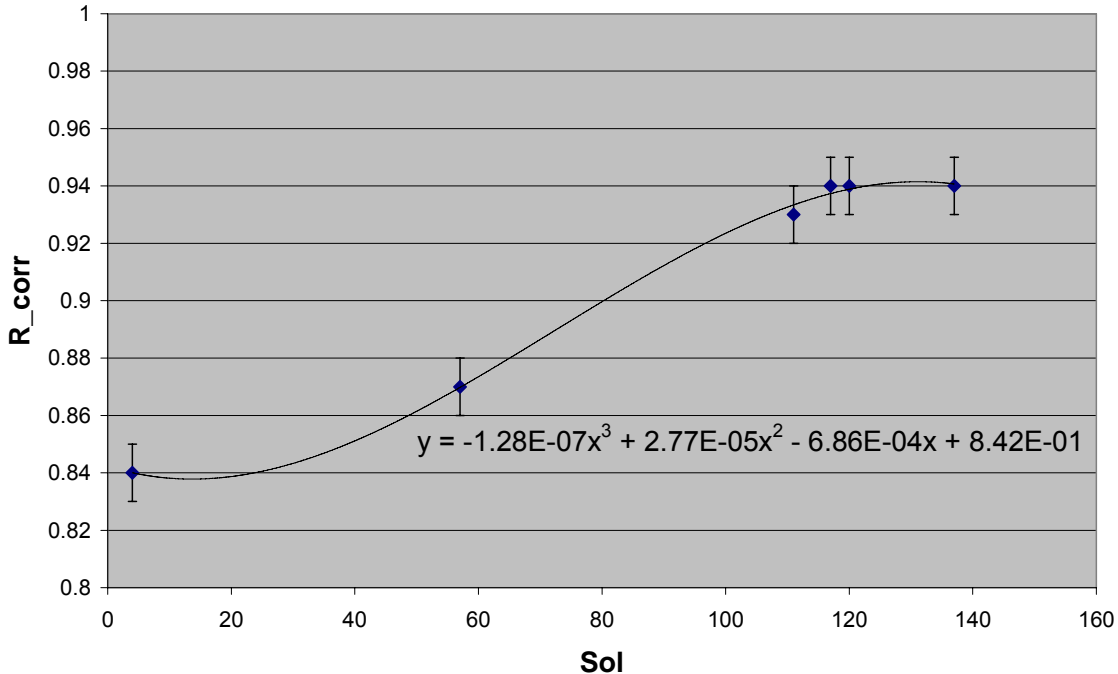
Figure 23. Red correction factor at -23 deg C. As the calibration for each of these sols was not always done at -23 deg C, we used the linear fit of Figure 22 to bring every data point at the midrange temperature, in order to determine g(t).

A degree-3 polynomial fit was used for modeling, as a linear approximation was evidently not adequate. Of course, it would have been better to have more data points, but we unfortunately realized a bit late that we had such variation. By experience, a human eye can not distinguish a difference of less than about 2% in the color composites, so the model seems reasonably accurate.

However, the fit is only valid until sol 137. For images taken after sol 137, we can assume that the correction is the same as sol 137, as it seems that a plateau was reached (same values between sol 120 and 137).

Figure 24 shows the final results, obtained with the linear interpolation of Figure 22 and the polynomial interpolation of Figure 23. In summary, the formulas used to determine the correction factors are:

R_corr = (2.40E-04*T + 2.12E-01) * (-1.28E-07*t3 + 2.77E-05*t2 - 6.86E-04*t + 8.42E-01) / 0.94
G_corr = 1.37E-04*T + 5.22E-01
B_corr = 1

where t = sol_number and T = OM CCD temperature (DN). **For sol > 137, use t=137.**
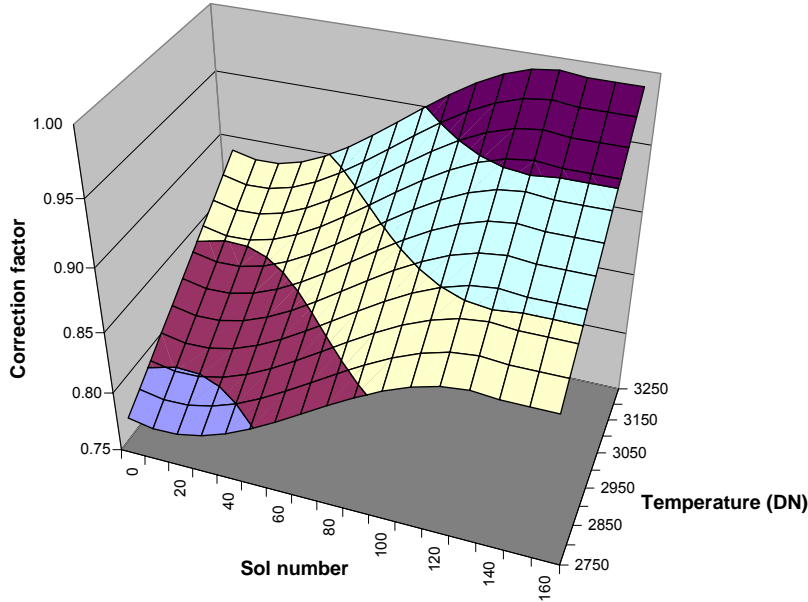
Figure 24. The correction factor for the red images, determined with the interpolations of figures 22 and 23.

IMPORTANT. Those correction factors were calculated for images taken with exposure durations proportional to red_exp = 275ms, green_exp = 200ms and blue_exp = 162.5ms. For sols 21 to 41, the red exposure duration was 1.22 times larger than expected, so the red correction factor for these sols should be divided by 1.22. Similarly, for sol 20, the red correction factor has to be divided by 1.5. The table hereafter shows the red correction factors that we need to apply to the flight images.

Sol & T (DN)	2750	2800	2850	2900	2950	3000	3050	3100	3150	3200	3250
0	0.78	0.79	0.80	0.81	0.82	0.83	0.85	0.86	0.87	0.88	0.89
10	0.78	0.79	0.80	0.81	0.82	0.83	0.84	0.85	0.86	0.87	0.88
19	0.78	0.79	0.80	0.81	0.82	0.83	0.84	0.85	0.86	0.87	0.88
20	**0.52**	**0.53**	**0.53**	**0.54**	**0.55**	**0.55**	**0.56**	**0.57**	**0.58**	**0.58**	**0.59**
21	**0.64**	**0.65**	**0.65**	**0.66**	**0.67**	**0.68**	**0.69**	**0.70**	**0.71**	**0.72**	**0.73**
30	**0.64**	**0.65**	**0.66**	**0.67**	**0.68**	**0.68**	**0.69**	**0.70**	**0.71**	**0.72**	**0.73**
41	**0.65**	**0.66**	**0.66**	**0.67**	**0.68**	**0.69**	**0.70**	**0.71**	**0.72**	**0.73**	**0.74**
42	0.79	0.80	0.81	0.82	0.83	0.84	0.85	0.87	0.88	0.89	0.90
50	0.80	0.81	0.82	0.83	0.84	0.85	0.86	0.88	0.89	0.90	0.91
60	0.81	0.82	0.83	0.84	0.85	0.87	0.88	0.89	0.90	0.91	0.92
70	0.82	0.83	0.84	0.86	0.87	0.88	0.89	0.90	0.91	0.92	0.93
80	0.83	0.85	0.86	0.87	0.88	0.89	0.90	0.91	0.93	0.94	0.95
90	0.85	0.86	0.87	0.88	0.89	0.90	0.92	0.93	0.94	0.95	0.96
100	0.86	0.87	0.88	0.89	0.90	0.91	0.93	0.94	0.95	0.96	0.97
110	0.86	0.88	0.89	0.90	0.91	0.92	0.94	0.95	0.96	0.97	0.98
120	0.87	0.88	0.89	0.91	0.92	0.93	0.94	0.95	0.97	0.98	0.99
130	0.87	0.88	0.90	0.91	0.92	0.93	0.94	0.96	0.97	0.98	0.99
140	0.87	0.88	0.89	0.91	0.92	0.93	0.94	0.95	0.97	0.98	0.99
150	0.87	0.88	0.89	0.91	0.92	0.93	0.94	0.95	0.97	0.98	0.99
160	0.87	0.88	0.89	0.91	0.92	0.93	0.94	0.95	0.97	0.98	0.99

III.   Atomic Force Microscope (AFM)

III.0. Overview

As shown in Figure 25, the MECA AFM is located between the OM and the SWTS inside the MECA enclosure. It scans a small region (from 1-65 µm square) on any of the 69 substrates, each positioned along the rim of the SWTS. Since the sample wheel can be rotated (but not elevated) prior to initiation of scanning, the AFM can access a thin band approximately 1/3 of the way up from the bottom of the corresponding OM image.

The AFM comprises three major components, a microfabricated probe-chip, an electromagnetically actuated scanner, and single board control electronics. The probe-chip features eight high aspect ratio silicon tips mounted on thin cantilevers, which are in turn mounted on sturdy silicon beams (Figure 26). The array geometry is designed to spread the resonant frequencies of the levers between 30 and 40 kHz in order to avoid cross-talk during dynamic operation. The force constant of the levers varies between 9 and 13 N/m.

Figure 25. Left: The AFM scanner viewed from the perspective of the sample. Right: The scanner positioned between the OM and the SWTS.
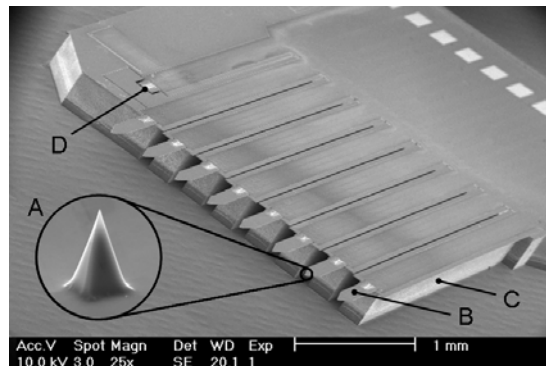

Figure 26. The AFM chip. (A) is a close-up of one of the silicone tips, (B) points is one of 8 cantilevers mounted on a cleavable support-beam (C). D) is a reference piezoresistor used for temperature compensation.

## III.1. Scanner Ground Calibration

Scanning is achieved using an electromagnetic actuator. Such an actuator does not require the high voltages of the more usual piezoelectric scanner and provides a large scan range of up to 65 µm for maximizing the resolution overlap between the OM and AFM. The z-axis servo signal represents the sample topography as the tip is rastered across the surface in the x (fast) and y (slow) directions.

For the actuation, three electrical coils are located underneath the suspended platform of the scanner head. The resistances of the FM coils were measured through the flexprint. The following values were obtained:

<center>

X coil: 479 Ω

Y coil: 478 Ω

Z coil: 483 Ω

</center>

The AFM chip is mounted on the suspended platform such as it has two orthogonal tilt angles of 10° relative to the sample to ensure that only one tip contacts the sample at a time. As shown in Figure 27, the X and Y axes of the MECA AFM image are rotated by +45° relative to the OM images.

It was noted at Imperial College that images produced by an AFM EM were flipped along the Y direction. This should also be the case for the FM.
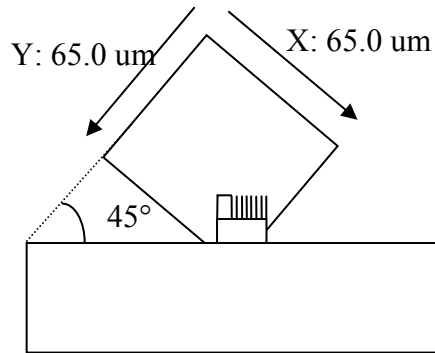
Figure 27. Geometry of the AFM scan field relative to the OM coordinate system (view from behind). The AFM scanning is at 45° relative to the OM axis. The field can be shifted laterally by rotating the SWTS in 15 µm increments.

The MECA AFM is capable of addressing areas up to 65 µm on a side in up to 512 x 512 pixels. Due to the properties of the scanner, the vertical range (or Z range) is dependent on the lateral size of the scan (XY range). If we assume that the full Z range is 13.80 microns (in fact 12 microns, see III.6.3), the Z range for each XY scanrange is given hereunder:

<pre>
        XY scanrange   Corresponding Z range
        65 um (Full Range)   ± 4.05 um ≡ 8.10 um
        50 um: ± 4.71 um ≡ 9.42 um
        40 um: ± 5.59 um ≡ 11.18 um
        20 um: ± 6.02 um ≡ 12.04 um
        10 um: ± 6.46 um ≡ 12.92 um
        5 um: ± 6.67 um ≡ 13.34 um
        2 um: ± 6.80 um ≡ 13.60 um
        1 um: ± 6.85 um ≡ 13.70 um
        0 um: ± 6.90 um ≡ 13.80 um (Full Range)
</pre>

Thus, the Z range of a 65um scan is about 8 microns. As a large Z range is needed to image particles, we expect to acquire scans with 10-30 μm on a side, typically contained in 256 x 256 "pixels" for a lateral granularity of ~0.1 μm/pixel.

The scanner is calibrated using settings of the AFM Control Software. For the FM, the following parameters were determined for a flat surface:

Signal mapping:

        X: +/- 33 um   (X scan range = 65 microns)
        Y: +/- 33 um   (Y scan range = 65 microns)
        Z: +/- 6.9 um   (Z scan range = 13.8 microns)

Slope corrections:

        X-Slope: - 0.0°
        Y-Slope: - 5.0°

Orthogonality corrections:

        XtoY: 0.0
        YtoX: 0.0

These settings were determined at room temperature. As mentioned in III.3, the scanrange at low temperature is decreased (about -30% at -30 deg C). In addition, it was observed that the vertical range calibration depends on the selected mode (static or dynamic), as well as on the feedback settings. Thus, in-situ measurements should be realized to calibrate properly the vertical range.

For those settings, the values of AxisUnitX, AxisUnitY and AxisUnitZ (for AxisSelect =0 and 1) to be used with AFM Control Software are:

ScanRange	65 um		40 um		30 um		20um		10um		5um	
AxisSelect	1	0	1	0	1	0	1	0	1	0	1	0
AxisUnitX	0	252	0	155	0	116	0	78	0	39	0	19
AxisUnitY	252	0	155	0	116	0	78	0	39	0	19	0
AxisUnitZ	-105	0	-65	0	-49	0	-32	0	-16	0	-8	0

III.2. Chip Ground Calibration

The AFM chip consists of 8 cantilevers ended by a sensor tip, plus a reference. Each cantilever features an integrated piezoresistive stress sensor, which is used to measure its pure deflection (static mode) or its vibration amplitude, frequency and phase (dynamic mode). The piezoresistors are addressed by a multiplexer, which links them to a temperature-compensated Wheatstone bridge. The bridge contains also the piezoressitor of the reference.

III.2.1. Electrical resistances of the stress sensors (in kΩ)

Lever 1:	On chip measurement: 3.37	Through flexprint measurement: 3.21
Lever 2:	On chip measurement: 3.44	Through flexprint measurement: 3.24
Lever 3:	On chip measurement: 3.45	Through flexprint measurement: 3.24
Lever 4:	On chip measurement: 3.42	Through flexprint measurement: 3.20
Lever 5:	On chip measurement: 3.45	Through flexprint measurement: 3.30
Lever 6:	On chip measurement: 3.45	Through flexprint measurement: 3.40
Lever 7:	On chip measurement: 3.47	Through flexprint measurement: 3.26
Lever 8:	On chip measurement: 3.53	Through flexprint measurement: 3.37
Reference:	On chip measurement: 3.61	Through flexprint measurement: 3.37

The capacity of the piezoelectric element, which provides the excitation for the cantilever array in dynamic mode, is 1.3nF.

III.2.2. Bridge Initialization

The following table shows that the values found for Bridge Offset after the initialization are independent of the voltage applied on the tip for the FM.

Bridge Offset [V]	Vtip = -5 V	Vtip = -3 V	Vtip = -1 V	Vtip = 0.5 V
Lever 1	-5.16	-5.16	-5.16	-5.16
Lever 2	-5.13	-5.13	-5.13	-5.13
Lever 3	-5.13	-5.13	-5.13	-5.13
Lever 4	-5.16	-5.16	-5.16	-5.16
Lever 5	-5.13	-5.13	-5.13	-5.13
Lever 6	-5.13	-5.13	-5.13	-5.13
Lever 7	-5.12	-5.12	-5.12	-5.12
Lever 8	-5.02	-5.02	-5.02	-5.02

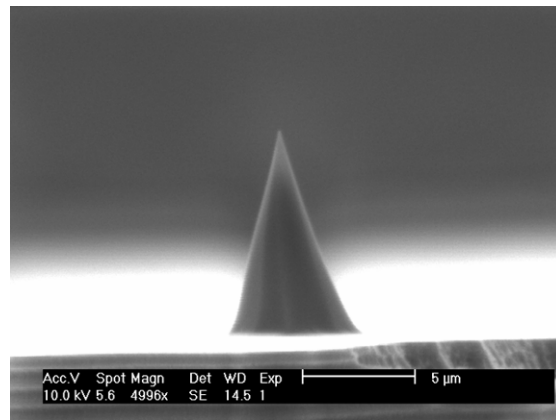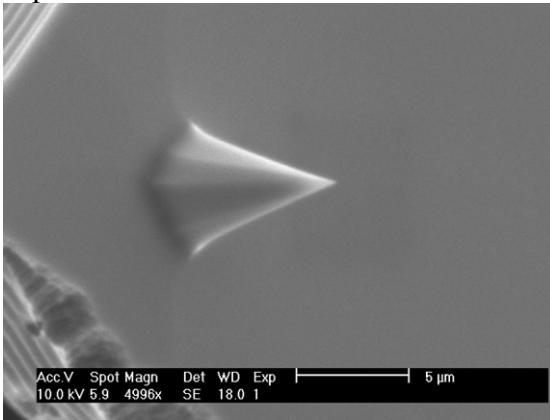The range for the voltage is [-10V; -4V], which corresponds to a DN range of [0; 255].

III.2.3. SEM images of the silicon tips

SEM images of the silicon tips were taken as a reference for the interpretation of the AFM images. For each tip, two sides views as well as a top view were taken.
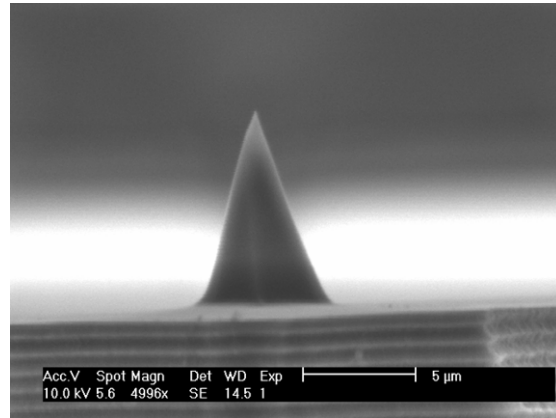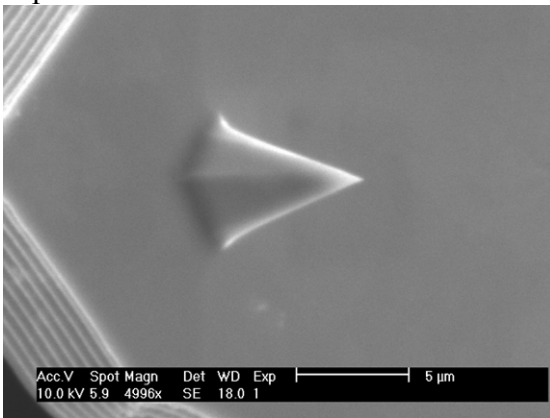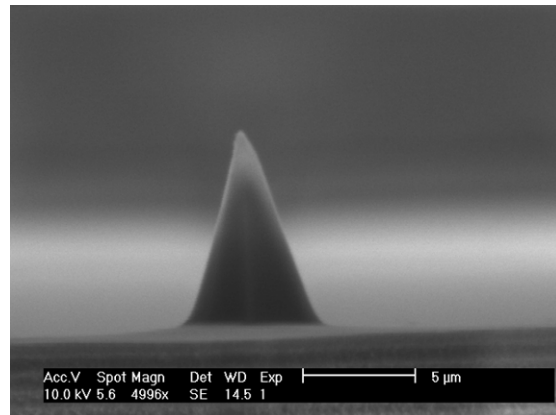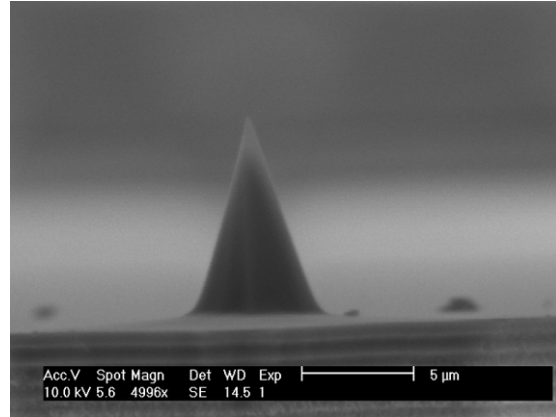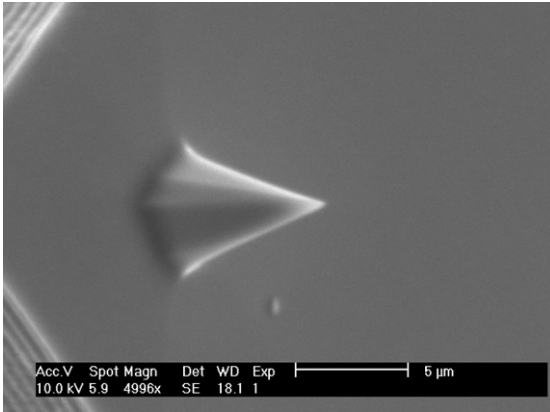
III.2.3.1. Side views

Tip n°1

Tip n°2

Tip n°3
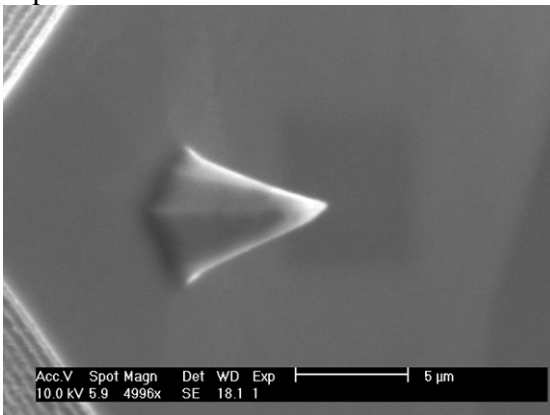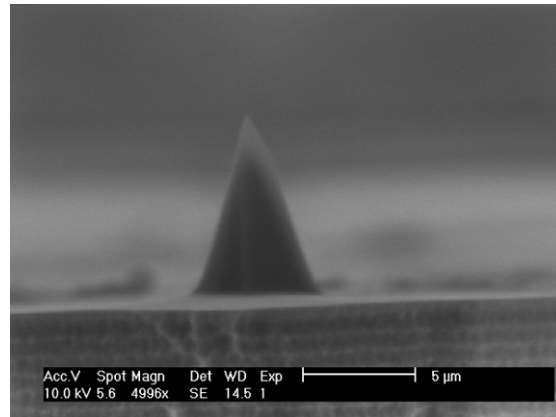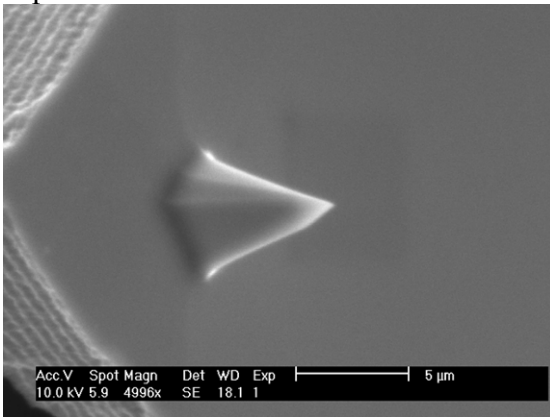
MECA Microscopy Calibration Report
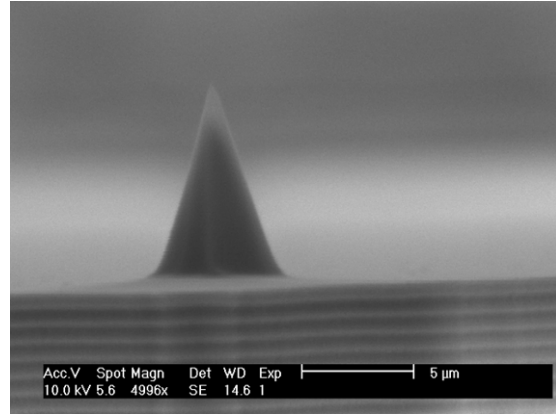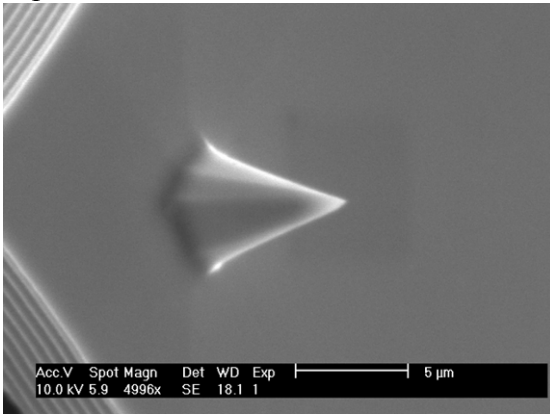
Tip n°4

Tip n°5
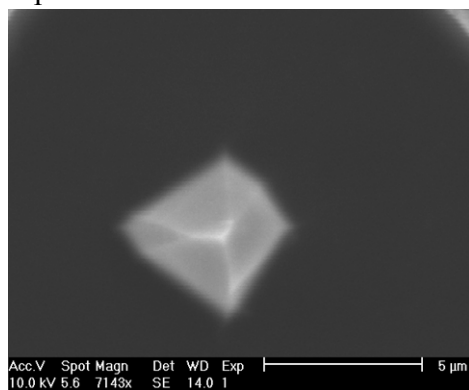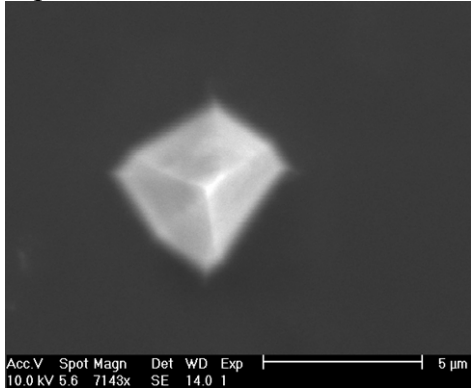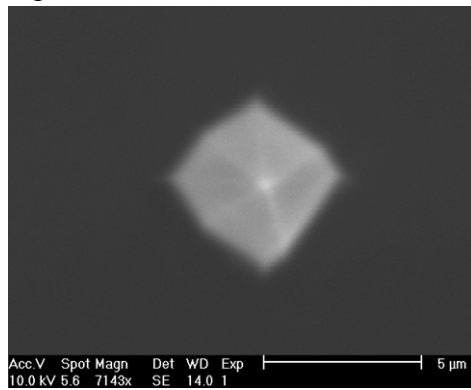
Tip n°6
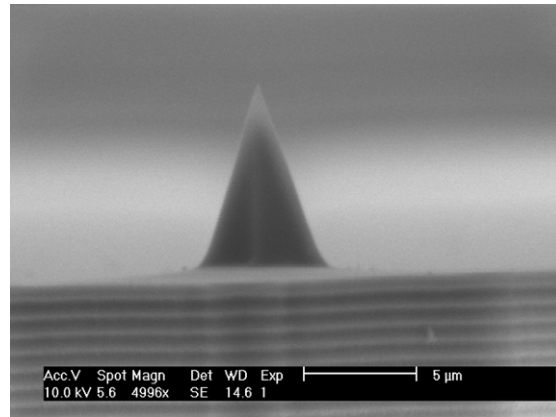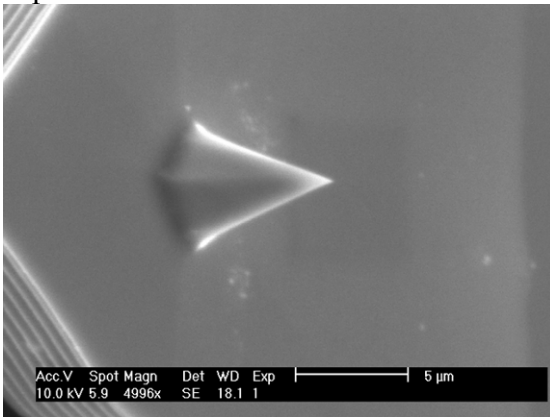
Tip n°7

Tip n°8

III.2.3.2. Top views

Tip n°1   Tip n°5
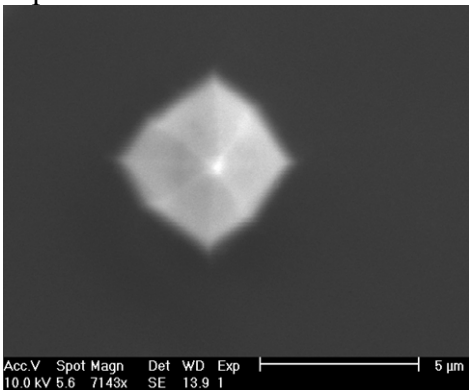
Tip n°2

Tip n°6

Tip n°3
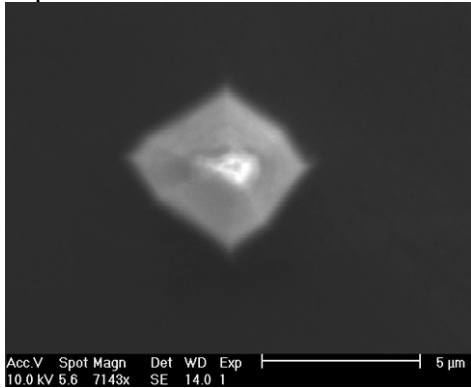
Tip n°7
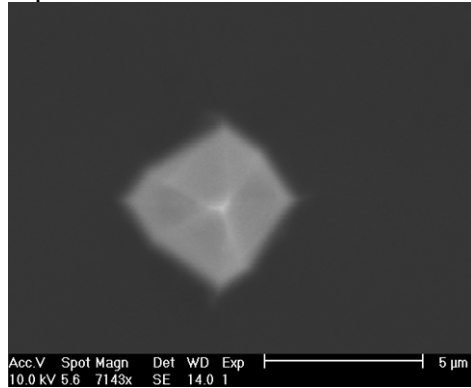
Tip n°4
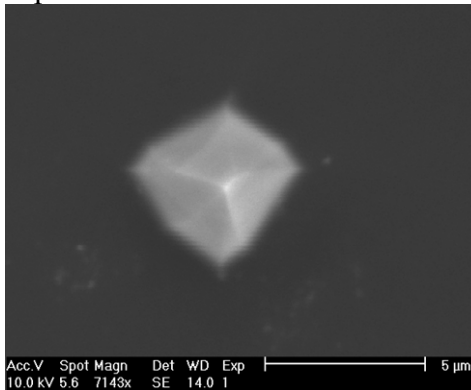
Tip n°8
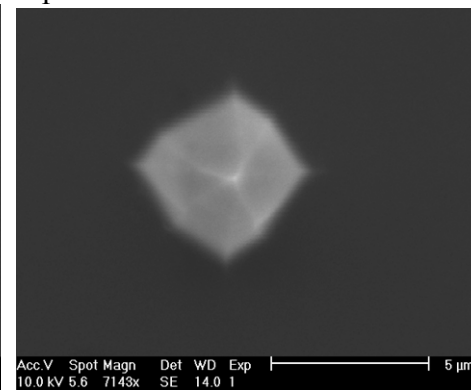
III.2.4. Resonance frequency of each cantilever

For the FM and the FS AFM, the resonance frequency (and the corresponding Vap, Vshake and phase) of each cantilever was determined at temperatures between -50°C to +20°C, under N_2 atmosphere, at a pressure of 5-10 mbar.

Remark: the oscillation can be maximal (i.e. Vap minimum) for different phase values.

T [°C]	Cantilever 1				Cantilever 2			
	fo [kHz]	Vap [V]	Vsh [V]	phase[°]	fo [kHz]	Vap [V]	Vsh [V]	phase[°]
23	38.255	0.41	1	40	33.449	0.25	1	100
20	38.260	0.37	1	60 40	33.454	0.29	1	100
15	38.277	0.70	-1	160	33.463	0.43	1	100
10	38.260 38.267	0.33 0.33	1 1	40 20	33.470	0.52	1	100
5	38.278	0.20	1	40 60	33.477	0.66	1	100
0	38.290	0.21	1	40 60	33.486	1.20	1	80
-5	38.300	0.23	1	40 60	33.479	0.59	1	100
-10	38.306	0.25	1	40 60	33.490	0.49	1	100
-15	38.312	0.27	1	40 60	33.497	0.51	1	100
-20	38.319	0.29	1	40 60	33.504	0.55	1	100
-25	38.325	0.33	1	40 60	33.510	0.59	1	100
-30	38.332	0.35	1	40 60	33.515	0.61	1	100
-35	38.338	0.37	1	40 60	33.520	0.65	1	100
-40	38.345	0.39	1	40 60	33.525	0.68	1	100
-45	38.350	0.41	1	40 60	33.532	0.72	1	100
-50	38.357	0.43	1	40 60	33.536	0.74	1	100

T [°C]	Cantilever 3				Cantilever 4			
	fo [kHz]	Vap [V]	Vsh [V]	phase[°]	fo [kHz]	Vap [V]	Vsh [V]	phase[°]
23	37.096	0.72	1	40	32.323	0.39	1	100
20	37.103	1.25	1	0	32.328	0.43	1	100
15	37.082	0.21	1	80	32.336	0.59	1	100
10	37.111	0.20	1	80	32.343	0.80	1	100
5	37.119	0.23	1	80	32.344	0.55	1	100
0	37.126	0.25	1	80	32.353	0.65	1	100
-5	37.134	0.28	1	80	32.361	0.74	1	100
-10	37.141	0.31	1	80	32.367	0.80	1	100
-15	37.147	0.34	1	80	32.372	0.86	1	100
-20	37.153	0.37	1	80	32.378	0.89	1	100
-25	37.159	0.39	1	80	32.383	0.97	1	100
-30	37.166	0.41	1	80	32.387	1.02	1	100
-35	37.172	0.43	1	80	32.393	1.05	1	100
-40	37.178	0.45	1	80	32.399	1.09	1	100
-45	37.184	0.47	1	80	32.405	1.12	1	100
-50	37.190	0.49	1	80	32.410	1.16	1	100

T [°C]	Cantilever 5				Cantilever 6			
	fo [kHz]	Vap [V]	Vsh [V]	phase[°]	fo [kHz]	Vap [V]	Vsh [V]	phase[°]
23	36.276	0.45	-1	120	31.326	0.46	1	100
20	36.279	0.31	-1	120	31.329	0.49	1	100
15	36.272	0.20	1	100	31.335	0.66	1	100
	36.274	0.20	1	80	31.337	0.66	1	120
10	36.280	0.24	1	100	31.341	0.71	1	100
	36.282	0.24	1	80				
5	36.288	0.28	1	100	31.345	0.68	1	100
	36.290	0.28	1	80				
0	36.297	0.35	1	100	31.351	0.75	1	100
	36.299	0.35	1	80				
-5	36.301	0.35	1	100	31.357	0.79	1	100
	36.302	0.35	1	80				
-10	36.308	0.38	1	80	31.364	0.84	1	100
-15	36.314	0.40	1	80	31.370	0.88	1	100
-20	36.320	0.43	1	80	31.377	0.97	1	120
-25	36.327	0.47	1	80	31.380	0.99	1	120
-30	36.334	0.50	1	80	31.387	1.02	1	100
					31.385	1.02	1	120
-35	36.340	0.51	1	80	31.391	1.04	1	100
-40	36.343	0.54	1	80	31.394	1.09	1	100
-45	36.346	0.60	1	80	31.398	1.14	1	100
-50	36.350	0.64	1	80	31.402	1.20	1	100

T [°C]	Cantilever 7				Cantilever 8			
	fo [kHz]	Vap [V]	Vsh [V]	phase[°]	fo [kHz]	Vap [V]	Vsh [V]	phase[°]
23	34.723 *	0.195	1	80	30.608	0.50	1	100
20	34.729 **	0.195	1	80	30.612	0.52	1	100
					30.613	0.52	1	120
15	34.743	0.33	1	80	30.619	0.78	1	100
	34.741	0.33	1	100	30.618	0.78	1	120
10	34.751	0.39	1	80	30.624	0.72	1	100
	34.749	0.39	1	100				
5	34.756	0.42	1	80	30.631	0.82	1	100
					30.629	0.82	1	120
0	34.763	0.50	1	80	30.636	0.87	1	100
					30.634	0.87	1	120
-5	34.769	0.55	1	80	30.641	1.00	1	100
	34.768	0.55	1	100	30.640	1.00	1	120
-10	34.777	0.63	1	80	30.646	1.03	1	100
	34.775	0.63	1	100	30.645	1.03	1	120
-15	34.783	0.70	1	80	30.651	1.08	1	100
	34.783	0.70	1	100	30.650	1.08	1	120
-20	34.790	0.80	1	80	30.656	1.14	1	100
	34.789	0.80	1	100	30.656	1.14	1	120
-25	34.794	0.89	1	80	30.663	1.20	1	100
	34.792	0.89	1	100	30.662	1.20	1	120
-30	34.800	1.4	1	80	30.667	1.23	1	100
					30.666	1.23	1	120
-35	34.807	1.7	1	80	30.674	1.29	1	100
-40	34.815	2.3	1	40	30.678	1.37	1	100
-45	34.820	4.3	-1	160	30.681	1.41	1	100
-50	34.826	1.5	-1	140	30.684	1.47	1	100
					30.682	1.47	1	120

* other possibilities:

T [°C]	fo [kHz]	Vap [V]	Vsh [V]	phase[°]
23	34.716	0.195	1	120
	34.72	0.195	1	100
	34.726	0.195	1	60
	34.729	0.195	1	40

** other possibilities:

T [°C]	fo [kHz]	Vap [V]	Vsh [V]	phase[°]
20	34.724	0.195	1	120
	34.726	0.195	1	100
	34.732	0.195	1	60
	34.735	0.195	1	40

III.3. AFM Ground Calibration Images

The lateral range of the AFM at room temperature was determined empirically to be 65µm square by scanning a standard calibration target (Multifunction Target 4X-20X from Max Levy Autograph, Inc.) with 10 µm spacing. The following images show FM AFM images taken at room temperature in static mode (1) and dynamic mode (2) and at low temperatures in dynamic mode (3). The scale specified for each image corresponds to the specified setting, and could be different from the real size of the image.

III.3.1. Images taken in static mode
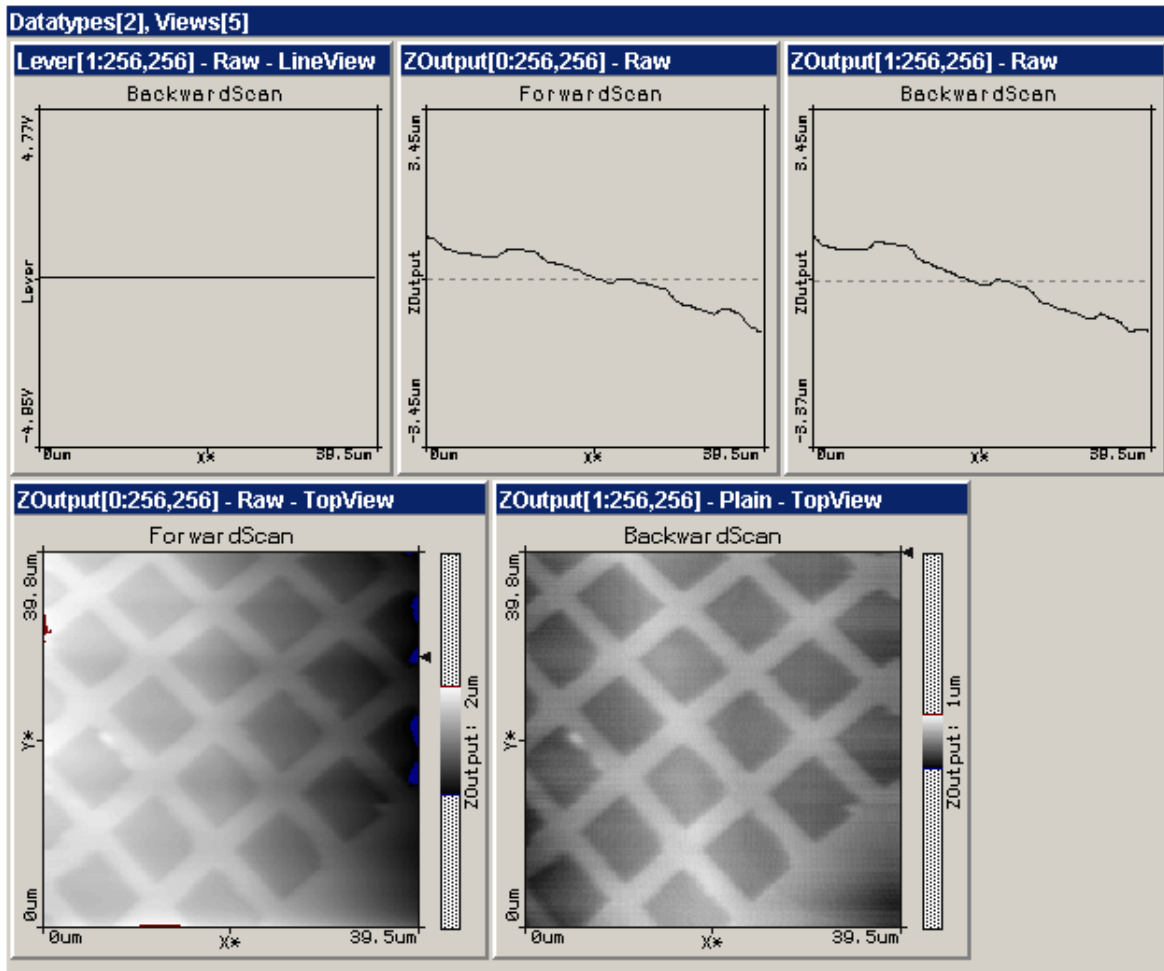
60 um image of the 10µm pitch calibration target
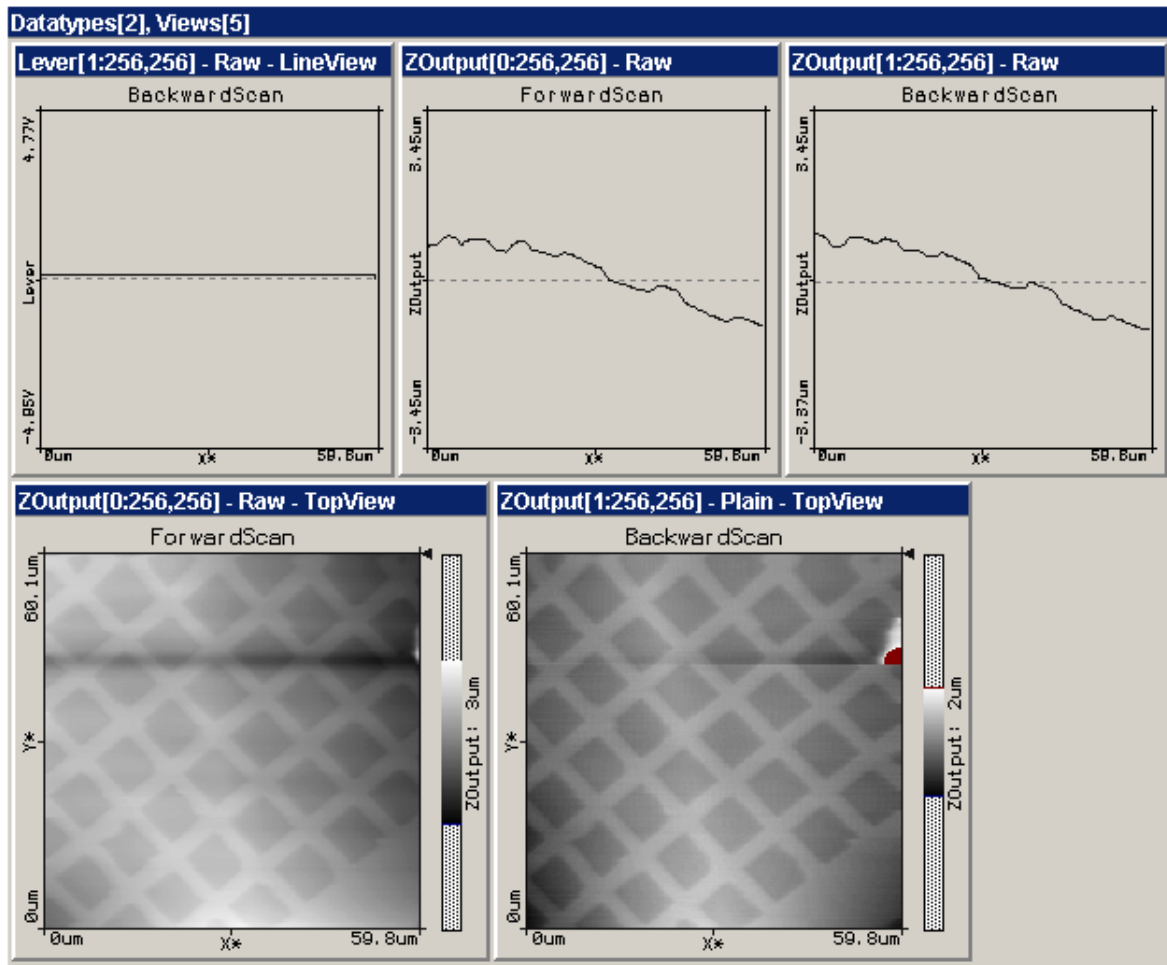
T = 23°C, P = 7 mbar

Scan parameters: time/line: 2.0 s
                    setpoint: -0.05 V
                    P-gain: 16
                    I-gain: 14

40 um image of the 10µm pitch calibration target
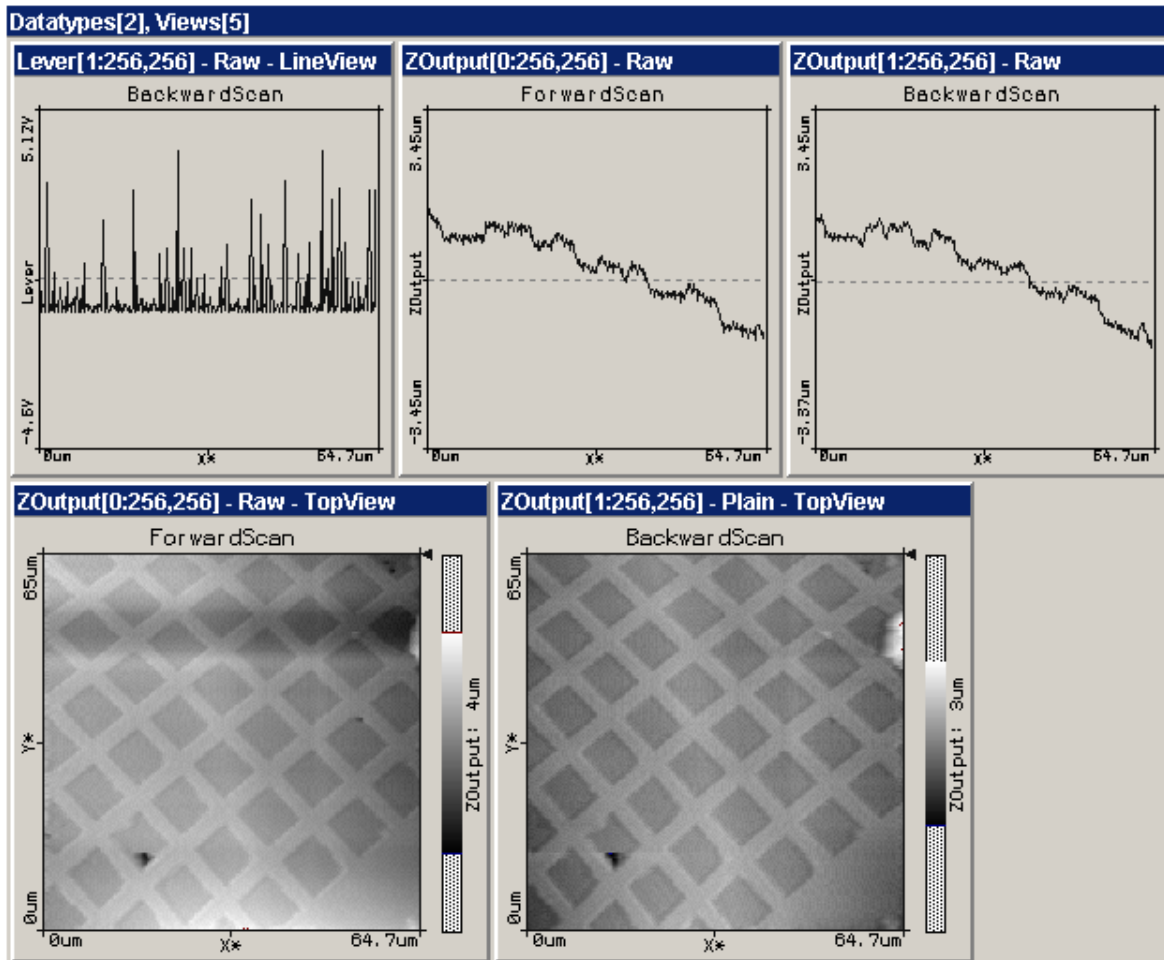

T = 29°C
P = 7 mbar

Scan parameters: time/line: 1.5 s
                    setpoint: -0.05 V
                    P-gain: 16
                    I-gain: 14

III.3.2. Images taken in dynamic mode

65 um image of the 10μm pitch calibration target

T = 20°C
P = 7 mbar

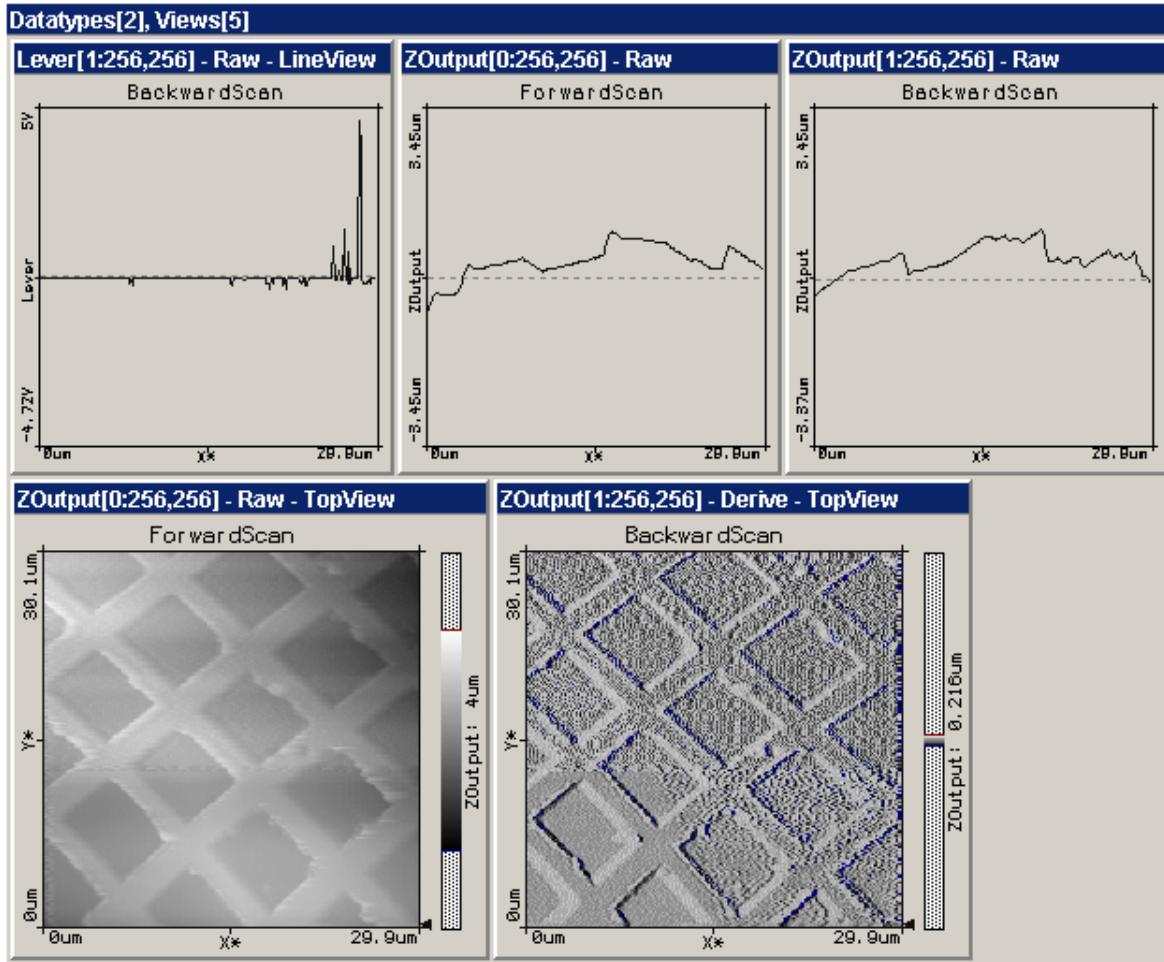Scan parameters: time/line: 2.4 s
                       setpoint: 0.3 V
                       P-gain: 9
                       I-gain: 9
                       PLL P-Gain: 0
                       PLL I-Gain: 3

30 um image of the 10μm pitch calibration target

T = 27°C to 28°C (from bottom to top)
P = 17 mbar

Scan parameters:
	time/line:	3.0 s (bottom) and 2.8 s (top)
	setpoint:	0.18 V
	P-gain:	10
	I-gain:	9
	PLL P-Gain:	1
	PLL I-Gain:	3

15 um image of the 10µm pitch calibration target

T = 29°C
P = 7 mbar

Scan parameters:

time/line:	3.5 s
setpoint:	0.25 V
P-gain:	6
I-gain:	10
PLL P-Gain:	0
PLL I-Gain:	3

III.3.3. Images at low temperature (in dynamic mode)

65 um image of the 10μm pitch calibration target
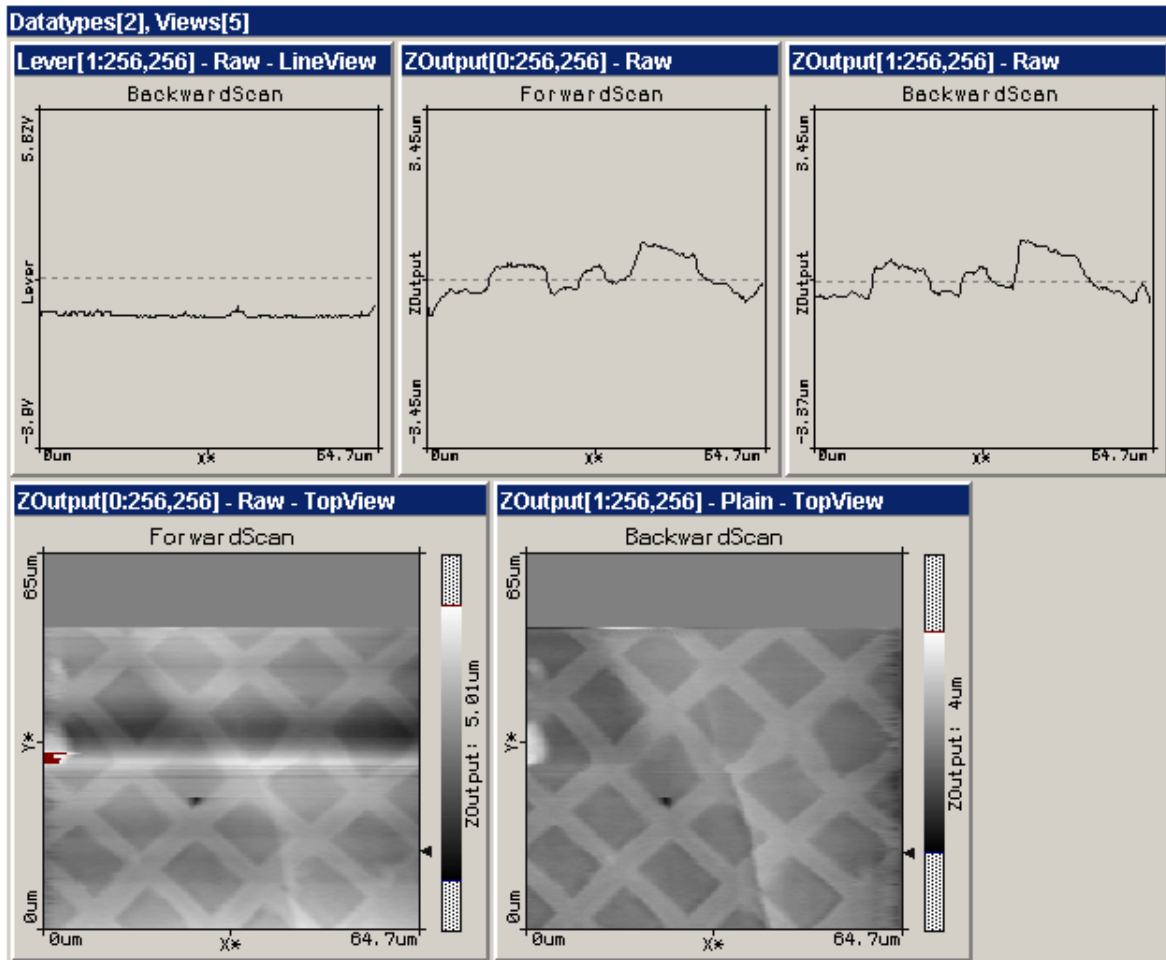
T = -19°C to -13°C (from bottom to top)
P = 6 mbar

Scan parameters: time/line: 1.8 s
                       setpoint: 1.0 V (approach : 2.0 V)
                       P-gain: 9
                       I-gain: 9
                       PLL P-Gain: 0
                       PLL I-Gain: 3

MECA Microscopy Calibration Report

65 um image of the 10μm pitch calibration target

T = -12°C ± 1°C
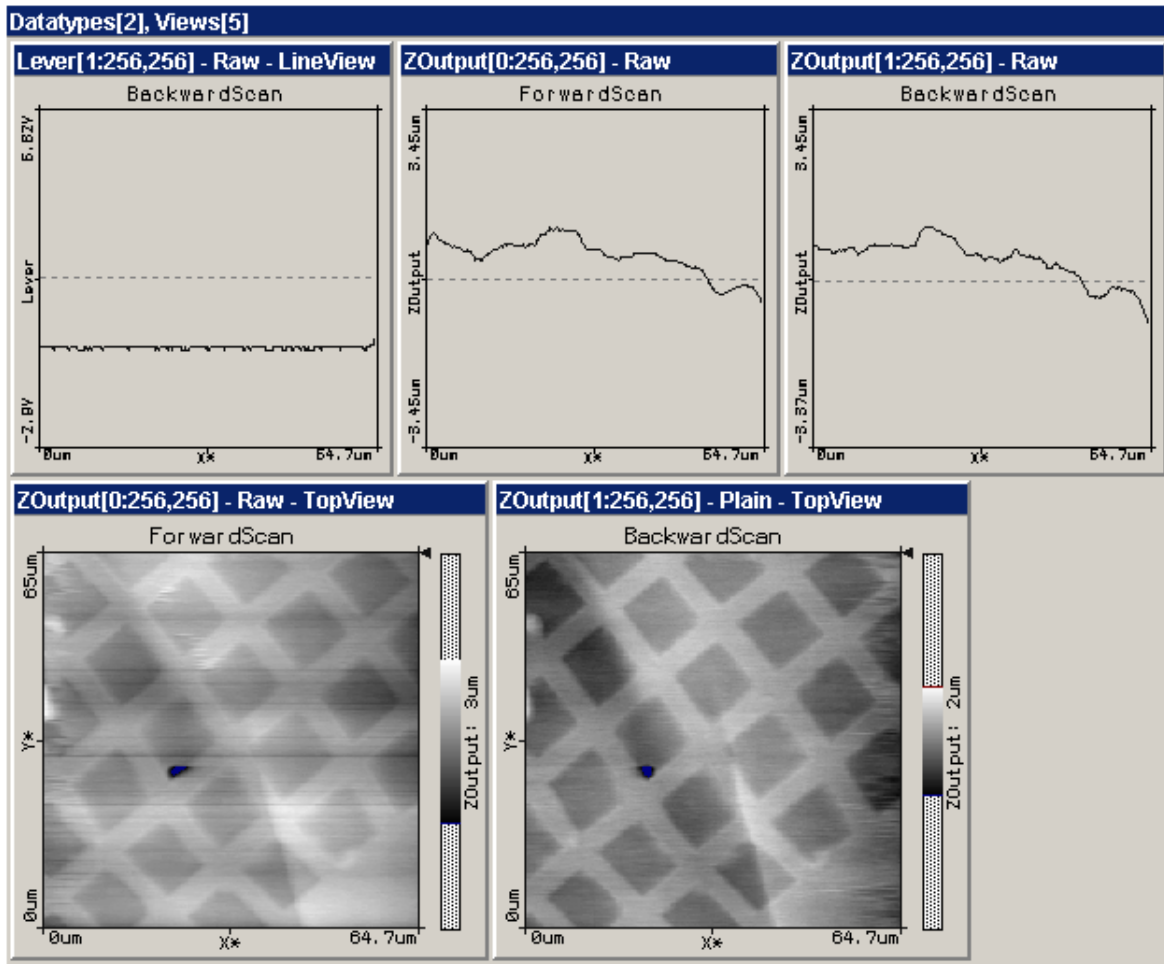P = 6 mbar

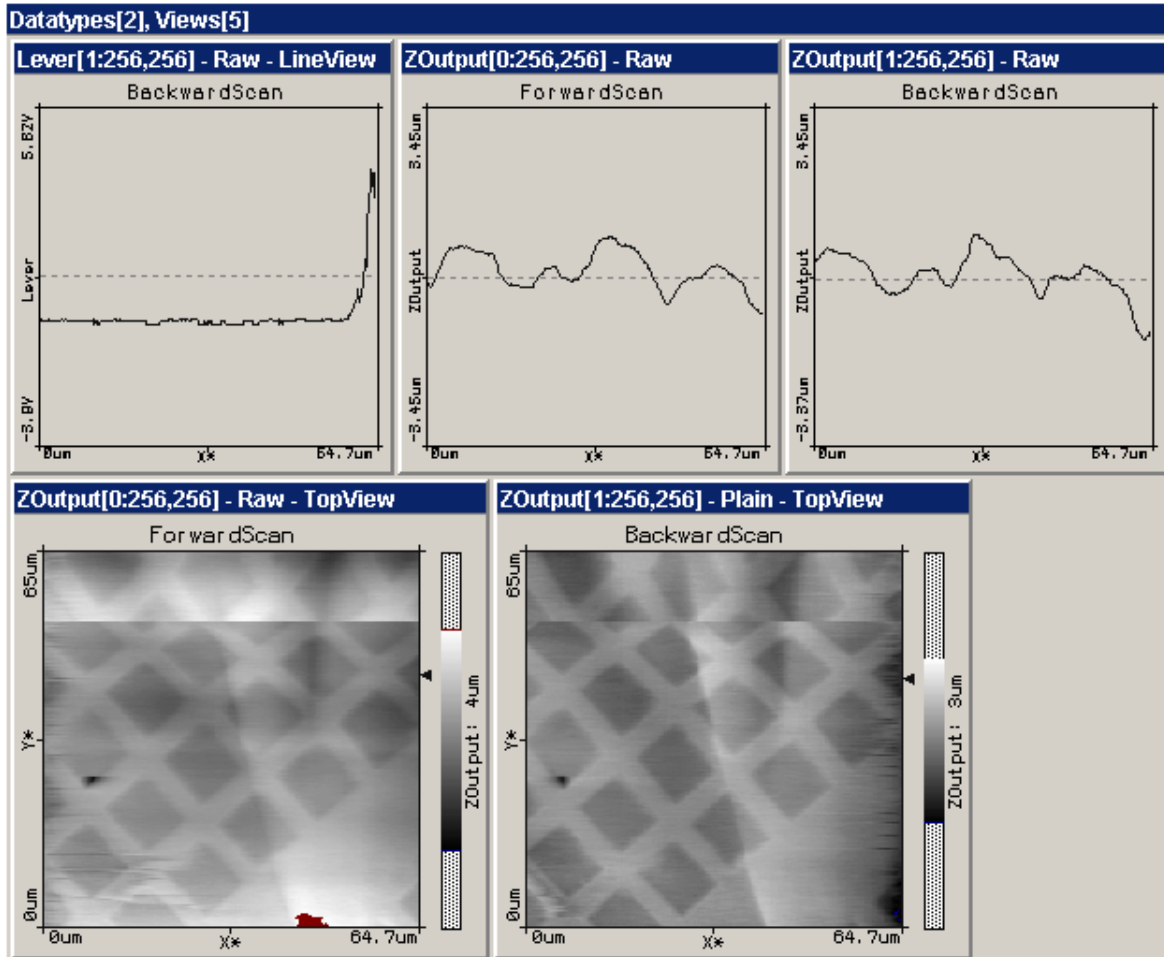Scan parameters: time/line: 1.8 s
                                      setpoint: 1.0 V (approach : 2.0 V)
                                      P-gain: 9
                                      I-gain: 9
                                      PLL P-Gain: 0
                                      PLL I-Gain: 3

65 um image of the 10µm pitch calibration target
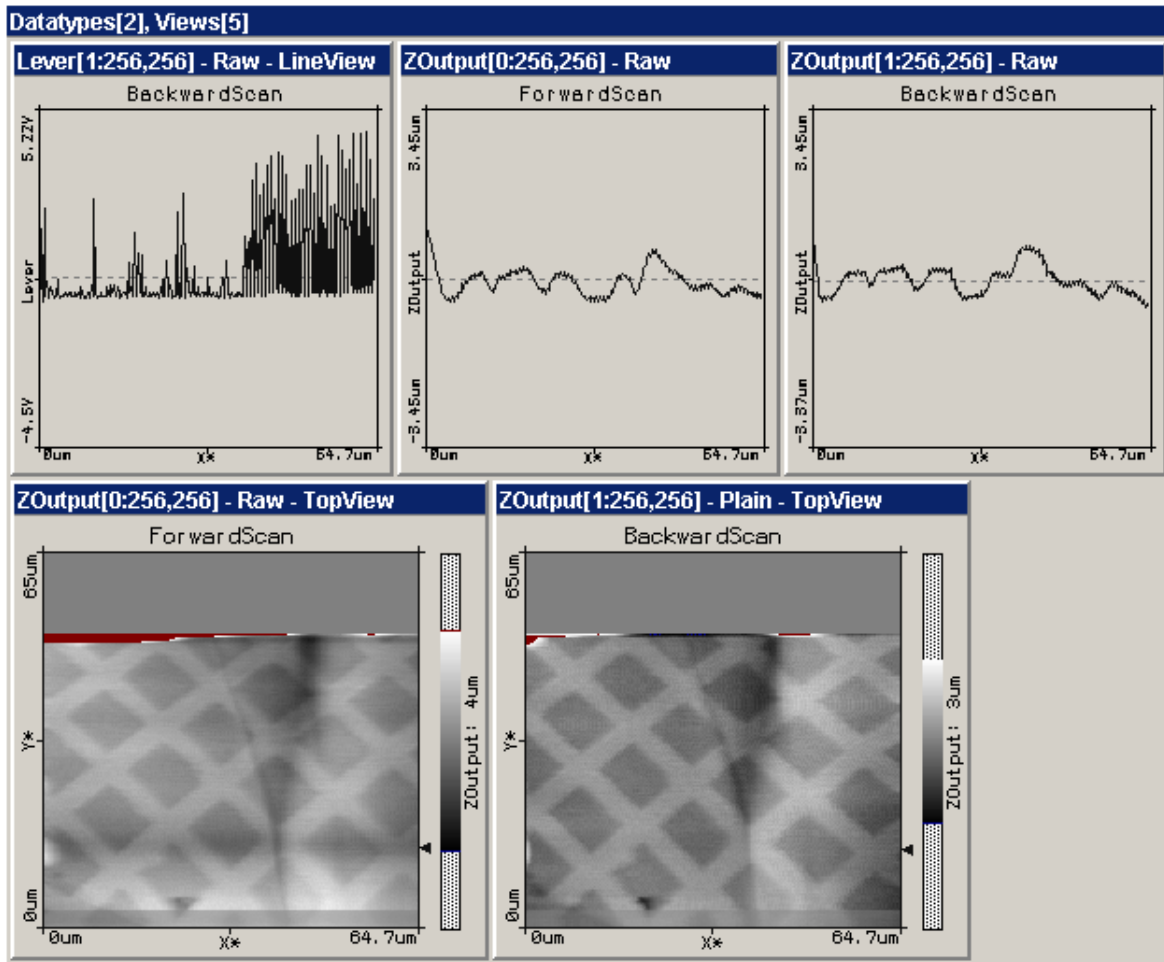

T = -3°C to 0°C (from bottom to top)
P = 6 mbar

Scan parameters:
time/line:	1.8 s
setpoint:	1.0 V
P-gain:	9
I-gain:	9
PLL P-Gain:	0
PLL I-Gain:	3

65 um image of the 10µm pitch calibration target

T = 0°C to 4°C (from bottom to top)
P = 6.5 mbar

Scan parameters:

time/line:	2.4 s
setpoint:	0.4 V
P-gain:	9
I-gain:	9
PLL P-Gain:	0
PLL I-Gain:	3

65 um image of the 10μm pitch calibration target

T = 4°C to 6°C (from bottom to top)
P = 6 mbar

Scan parameters:
time/line:	2.4 s
setpoint:	0.4 V
P-gain:	9
I-gain:	10
PLL P-Gain:	0
PLL I-Gain:	3

65 um image of the 10μm pitch calibration target
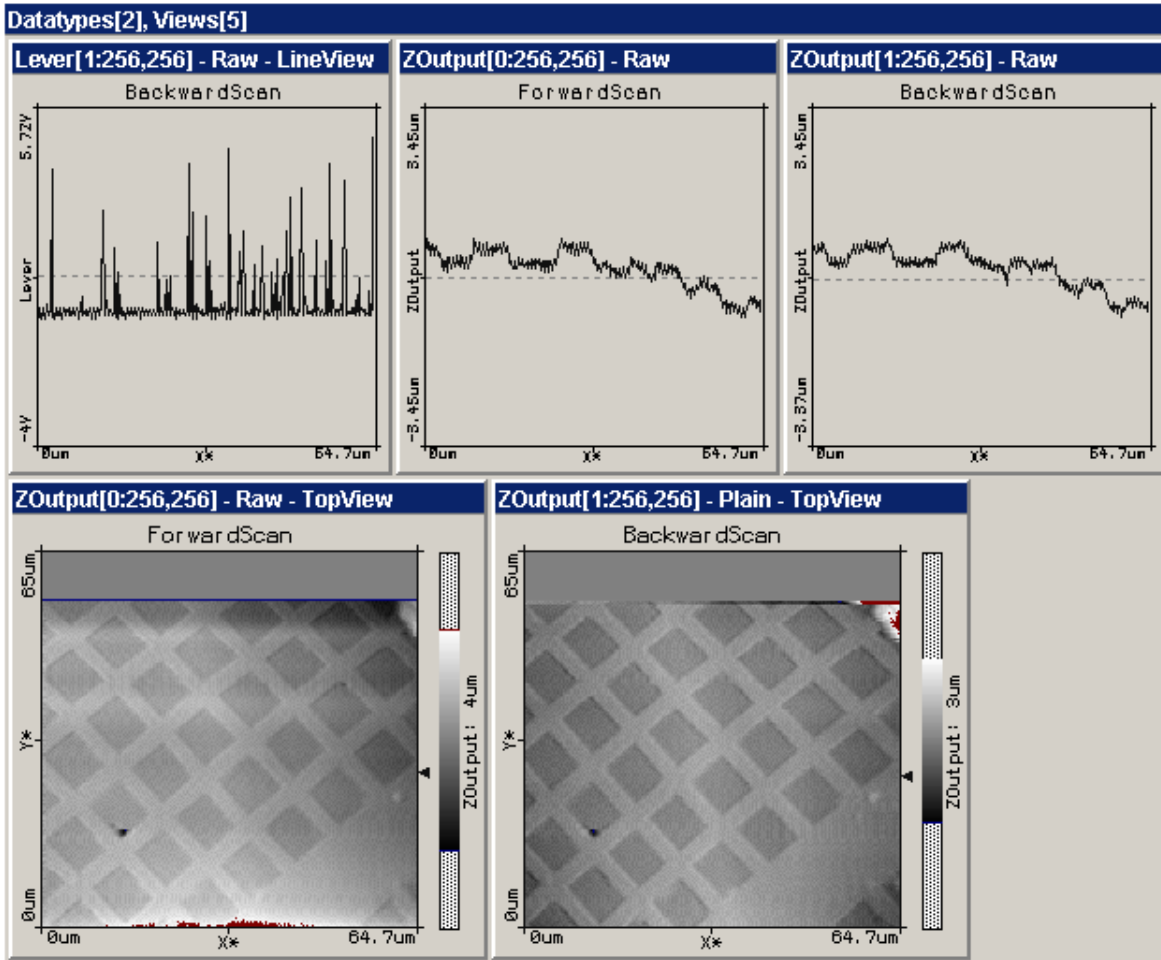
T = 17°C, P = 6 mbar

Scan parameters:	time/line:	2.3 s
	setpoint:	0.9 V
	P-gain:	9
	I-gain:	9
	PLL P-Gain:	0
	PLL I-Gain:	3

These images show that some distortions appear in the images at low temperature. As an AFM image takes almost one hour to be performed, the contribution of drifts on that time scale could be important. Such drifts are typically originating from changing temperatures, temperature gradients and different thermal expansion coefficients. The influence of thermal drift should be measured on flight-like testbeds (see III.5).

III.4. Scan Parameters for Static and Dynamic Mode

Remainder:

In static mode, the deflection signal is proportional to the force, which the microprocessor holds constant at a designated setpoint by adjusting the distance to the sample.

In dynamic mode, the resonant frequency of the cantilever is excited by a phase locked loop and the shift of the resonance frequency provides a measure of the force gradient. The microprocessor holds the resonance frequency at a designated setpoint by changing the distance to the sample.

Due to the different working principles, the settings are totally different for the two modes. The two following sections give the default settings for the FM, based on the previous images. A third section describes the possible choices for the vertical range.

III.4.1. Dynamic mode

Scan settings:	3.5 s /line ***
	256 points / line
	forward and backward scan

Feedback loop settings:	setpoint:	1.0V
	Pgain:	9
	Igain:	8
	TipVoltage:	-4 V

PLL loop settings	PLL Gain:	0
	PLL I Gain:	3

III.4.2. Static mode

Scan settings:	2.0 s/line ***
	256 points / line
	forward and backward scan

Feedback loop settings:	setpoint:	-0.05V
	Pgain:	16
	Igain:	14 (15)
	TipVoltage:	-4 V

*** In order to limit the number of particles displaced by the AFM tip, the scan speed should not exceed 5 um/s (test performed at Imperial College). Thus, the scan speed for a 40 um scan should theoretically not exceed 8.0 s/line.

III.4.3. Vertical Range

The AFM spans the full range of topography (~12 µm) in the vertical direction by encoding a fraction of that range in 8 bits, or 256 DN (+**127 means a deflection towards the surface**). The fraction is set by a commandable channel gain such that 0 spans the entire range and each subsequent increment reduces that range by a factor of two. Thus the maximum channel gain setting of 8 restricts each line scan to 1/256 of the available 12µm, or 47 nm (the centroid is adjusted after each line). That range is spread across 8 bits (256 DN) such that 1 DN corresponds to 0.18 nm, allowing a factor of 5 margin for drift and calibration changes. As an example of the influence of the gain setting, Figure 21 compares two images of the same region using gain settings 0 and 1. In practice, it is not expected that gains higher than 2 will be utilized during the mission.
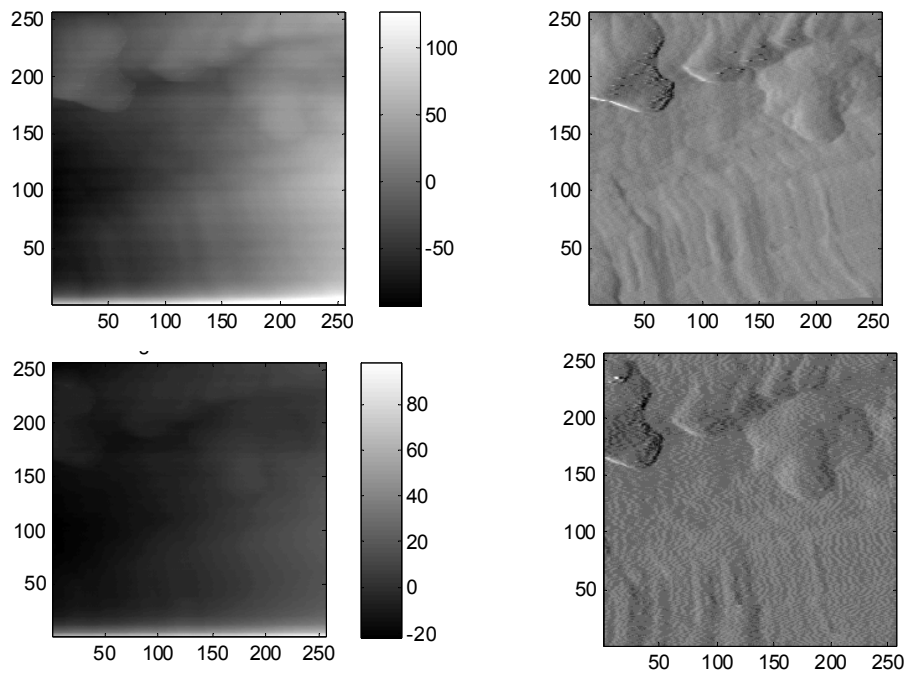
Figure 28. 256x256 AFM scans of a section of the anodized aluminum sample wheel, acquired at the PIT on Dec. 7, 2006, comparing the selection of different channel gains. Both scans are of a field 10µm on a side acquired at a speed of 3.5 s/line. The left-hand images are the raw topography, right hand are line-by-line derivatives, which better simulate what the eye would see if these were macroscopic, illuminated surfaces. Top: Channel gain = 0 (vertical step size 47 nm). Bottom: Channel gain = 2 (vertical step size 12 nm).

III.5. Pre-Launch Parameters

III.5.1. Thermal drift of the Test-Bed

Thermal drift can be found in the SWTS and the AFM scanner. Only the relative drifts between these two units are of importance. The most critical drift is in x_3 [or z-direction i.e. the direction perpendicular to the substrate's surface], next is the slow scan axis x_2, followed by the fast scan axis x_1.

Required input:
Expected temperature profile inside the MECA enclosure as function of time. Depending on the time scale of temperature variation compared to the time scale of 30-60 minutes a steady state or a dynamic situation must be assumed for a single scan.

Nested scans will last longer and there may be *operational* constraints, i.e. the sample-to-tip separation may drift out of the z-scan range.

Calibration procedure:
Measuring the 2D calibration grid at different temperatures and expected temperature changes in the test-bed. This will provide *typical* values for $\partial x_i / (\partial T\, \partial t)$. The typical values are important for *planning operations*. It is expected that general thermal behavior of the FM and EM are comparable. It is known, however, that the FM scanner has a particular distortion around 0 degree Celsius (c.f. data sheet). The actual values for the FM, which are relevant for interpreting the experimental data, can only be acquired on Mars during the *in-situ calibration*.

III.6. In-situ Calibration

There are three types of in-situ calibrations foreseen, first a detailed calibration campaign in the beginning of the mission and, second, a short calibration measurement during actual AFM operations. The third method will only be applicable for the nano-bucket substrate in case of sparse particle coverage and for reverse imaging of a contaminated tip. In those two cases there will be a (x,y) - standard visible in the AFM image, which will permit to absolutely calibrate the measurement. Calibration in z could be possible in case of the nano-bucket substrate.

III.6.1. Calibration Substrates

III.6.1.1. AFM Linear Calibration Substrate

A regularly spaced precision grid (see I.4.5) is used to establish the relationship between the commanded coordinates and actual coordinates, correcting for the characteristic saddle distortion and shrinkage of the overall scan range as temperatures are lowered. Even with a prior laboratory calibration, the actual sample temperature will not be known, and significant variation will also result from temperature gradients or temperature drift. As a result, frequent in-situ calibration is the only reliable method of correcting images to compensate for instrument artifacts such as saddle distortion. The

square pattern should also feature a defined height between the square holes and the square mesas. This is used to calibrate the z axis.

III.6.1.2. AFM Standard Calibration Substrate

A pincushion calibration grid (see I.4.6) is used to determine the shape of the AFM tip itself. An AFM image is a dilation of the shape of the substrate and the tip shape, a property that can change as tips become contaminated with dust or become dull due to micro-fracture and wear. Moreover, only the first of the eight available tips can be calibrated prior to its use, so the tip shape can only be determined when the previous beam is broken off. Thus, like the distortion correction, tip shape must be determined regularly in situ.

Tip wear was studied at the University of Neuchatel by repeated imaging of the pincushion array by a test tip. Figure 29 shows the gradual degradation of AFM scans at various stages, and Figure 30 shows the worn tip itself as imaged by a scanning electron microscope after 90 scans.
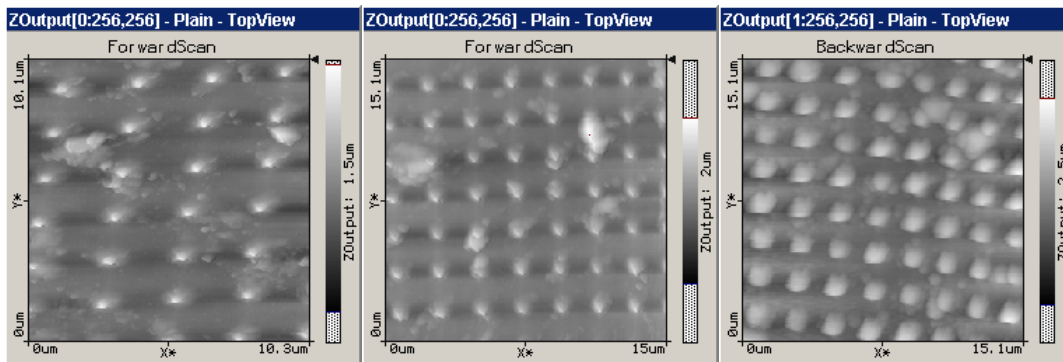

Figure 29. AFM image of "pincushion" with tip 4. Left: Scan 1. Middle: Scan 30. Right: Scan 80.
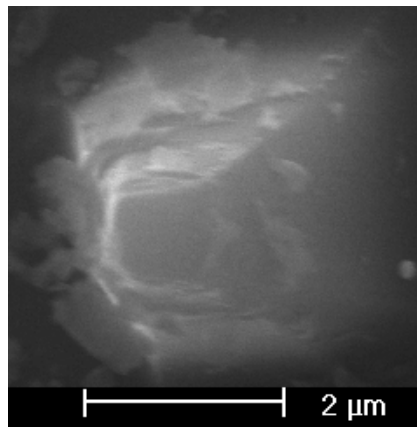

Figure 30. SEM image of tip 4 after 90 scans showing debris and minor blunting.

III.6.1.3. Tip Finder Tool

A third calibration substrate, the tip finder (see I.4.7), is used to associate each AFM tip position with the corresponding optical microscope field, making it possible to use the AFM to obtain a high resolution image of a structure of interest. Using silicon microfabrication techniques, the tip-finder is encoded with unique raised structures on a micron scale such that an AFM image of any portion is unique and recognizable. Since the AFM tip array has a precise, fixed shape, in situ use of the tip-finder should not provide any new information. It has been included in the calibration suite in the unlikely event that macroscopic translations occur due to vibration or mechanical failure of the AFM sample train.
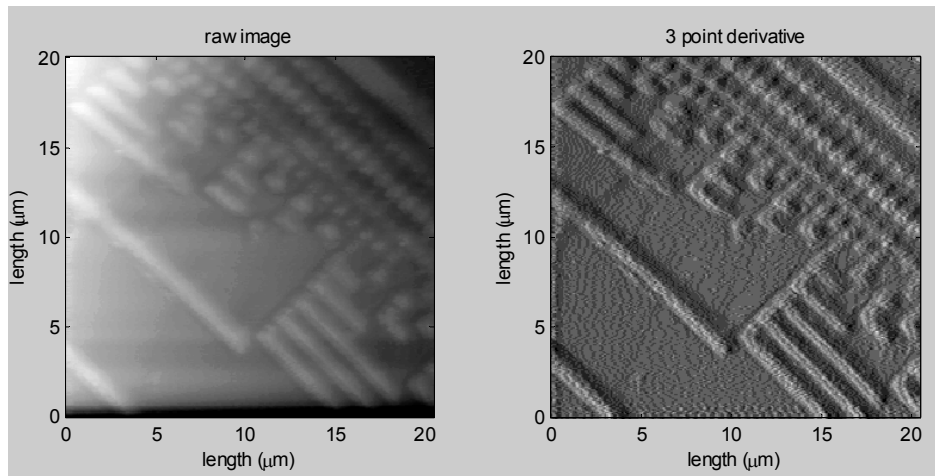
Figure 31. 20 x 20 μm AFM scan of the tip-finder substrate using channel gain 1 (corresponding to a 6.9 μm vertical range).

III.6.2. Calibration Procedure

During the health check in the early mission, the AFM will take several images of the three calibration substrates. The calibration data will be transmitted to Earth, where it will be used to calibrate the experimental AFM data.

Prior, in-between and at the end of AFM experiments, measurements on the calibration targets will be conducted. This serves two purposes: first the assessment of the tip shape and second the verification of the x,y calibration. The possibility of measuring the square patterns is also kept, the sequence being sufficiently flexible.

During all measurements, the temperature of the thermocouple will be registered in order to assess thermal drifts.

III.6.3. Calibration results

Several images of the calibration substrates were taken on Mars. On sol 100, three large and good images of the linear calibration substrate were taken and used to determine the x-y calibration of the scanner. Figure 32 shows how the largest image of the calibration grid was corrected using a polynomial transformation. This transformation was found by matching the intersections of the grid in the image with a perfect grid (3-micron period). Then, using the least squares method, the transformation sending "the best" the intersection points onto the new points was found, and applied to the other data points. Note that the pixels in the corrected image are not aligned on a grid.
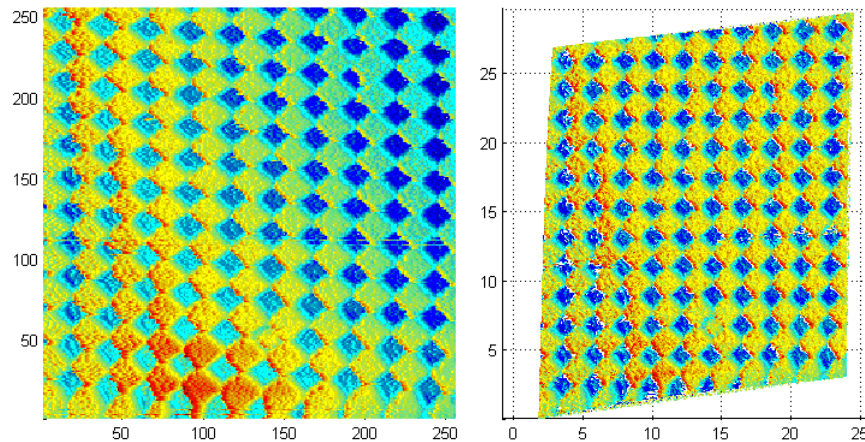
Figure 32. Left) Image of the linear calibration substrate (with a commanded scanrange of 35 microns). Right) Image calibrated and corrected for x,y and z distortions, using degree-3 polynomial transformation

The found transformation can be applied to AFM images of unknown samples to correct the non linear distortions. If those images are smaller than 35 microns, only a part of the transformation is used. If they are larger, the correction of the "exceeding" borders is not possible, or at least not very reliable.

In order to get a simpler model, the transformation can be replaced by two amplification factors, one for the x axis and another for the y axis. Based on the images taken on sol 100, those factors are:

x correction factor = 0.612 ± 0.015
y correction factor = 0.733 ± 0.005

For example, a commanded scan of 50 microns produces in fact a 30×36-μm scan.

The effective scanrange of the scanner depends on the temperature. Using the images taken prior to the flight (see III.3.3), the relation between the effective scan size and the temperature could be established (see Figure 33). For the range of temperatures seen during the operations, the scan area can be considered constant for a given commanded

scanrange. Thus, the polynomial transformation and the correction factors mentioned above can be used for all images, assuming that the properties of the scanner have not changed too much during the mission.
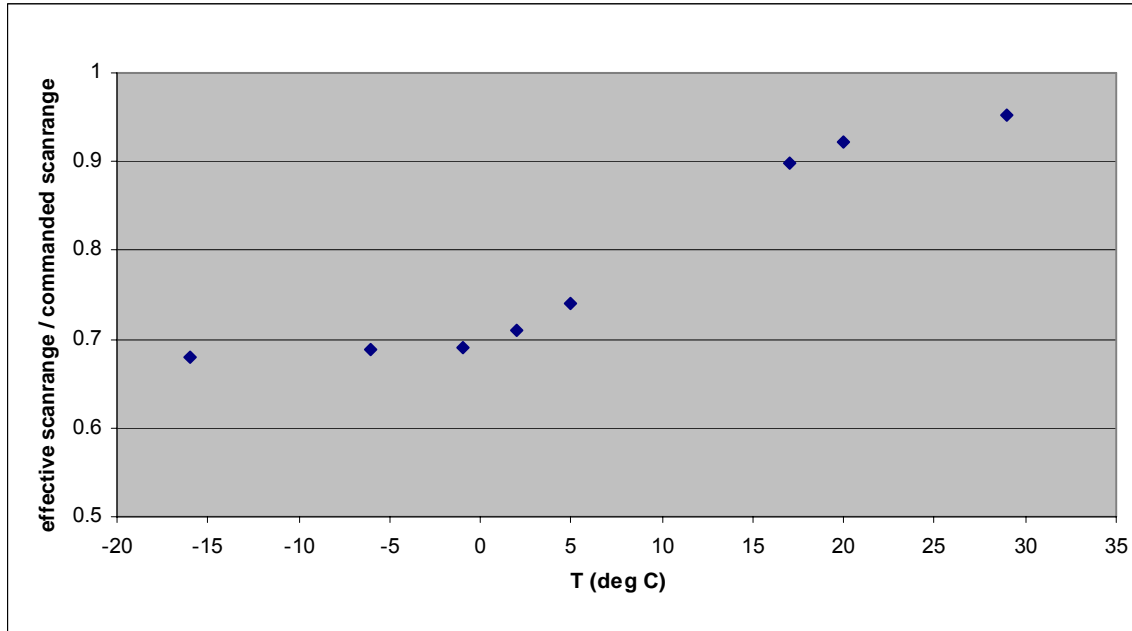

Figure 33. Amplification factor for the scanrange, determined based on pre-flight images. Note that the values at low temperature are constant, and close to the amplification factors found by means of the images of sol 100.

The calibration of the z range was determined by looking at pre-flight and Mars images of known structures. For the topography signal (with channel gain = 0), **the full z range of the scanner is 12 microns**, with an error of about ± 1 micron. As for the two other axes, this can be considered constant at the operations temperatures.

Finally, information was sometimes recorded in the error signal. As the relation between the shift in frequency and the tip-sample distance is not linear, it is not straightforward to calibrate the error channel. However, efforts could be made to find an approximation by looking at the second image of sol 91, where the information on a particle was recorded in both channels. This has not yet been done.